REINFORCED CONCRETE MODELING

H. L. Schreyer
J. W. Jeter, Jr.
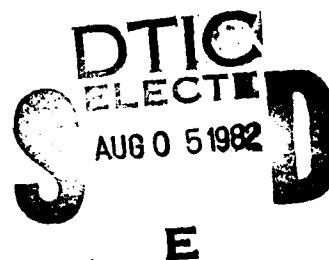
New Mexico Engineering Research Institute
University of New Mexico
Albuquerque, NM 87131

July 1982

Final Report

DTIC
ELECTE
AUG 0 5 1982
S   E

AIR FORCE WEAPONS LABORATORY
Air Force Systems Command
Kirtland Air Force Base, NM   87117

82 08 05 083

This final report was prepared by the New Mexico Engineering Research Institute, University of New Mexico, Albuquerque, New Mexico, under Contract F29601-81-C-0013, Job Order 88091347 with the Air Force Weapons Laboratory, Kirtland Air Force Base, New Mexico. Mr. Douglas R. Seemann (NTES) was the Laboratory Project Officer-in-Charge.

This report has been reviewed by the Public Affairs Office and is releasable to the National Technical Information Service (NTIS). At NTIS, it will be available to the general public, including foreign nations.

If your address has changed, if you wish to be removed from our mailing list, or if your organization no longer employs the addressee, please notify AFWL/NTES, Kirtland AFB, NM 87117 to help us maintain a current mailing list.

This technical report has been reviewed and is approved for publication.

DOUGLAS R. SEEMANN
Project Officer

FOR THE COMMANDER

RICHARD H. JOLLEY
Major, USAF
Chief, Technology Applications Branch

MAYNARD A. PLAMONDON
Chief, Civil Engrg Rsch Division

REPORT DOCUMENTATION PAGE		READ INSTRUCTIONS BEFORE COMPLETING FORM
1. REPORT NUMBER AFWL-TR-82-9	2. GOVT ACCESSION NO. AD-A117 925	3. RECIPIENT'S CATALOG NUMBER
4. TITLE (and Subtitle) REINFORCED CONCRETE MODELING		5. TYPE OF REPORT & PERIOD COVERED Final Report
		6. PERFORMING ORG. REPORT NUMBER NMERI TA8-9
7. AUTHOR(s) H. L. Schreyer J. W. Jeter, Jr.		8. CONTRACT OR GRANT NUMBER(s) F29601-81-C-0013
9. PERFORMING ORGANIZATION NAME AND ADDRESS New Mexico Engineering Research Institute University of New Mexico Albuquerque, NM 87131		10. PROGRAM ELEMENT, PROJECT, TASK AREA & WORK UNIT NUMBERS 62601F/88091347
11. CONTROLLING OFFICE NAME AND ADDRESS Air Force Weapons Laboratory (NTES) Kirtland Air Force Base, NM 87117		12. REPORT DATE July 1982
		13. NUMBER OF PAGES 90
14. MONITORING AGENCY NAME & ADDRESS(if different from Controlling Office)		15. SECURITY CLASS. (of this report) Unclassified
		15a. DECLASSIFICATION DOWNGRADING SCHEDULE

16. DISTRIBUTION STATEMENT (of this Report)

Approved for public release; distribution unlimited.

17. DISTRIBUTION STATEMENT (of the abstract entered in Block 20, if different from Report)

18. SUPPLEMENTARY NOTES

19. KEY WORDS (Continue on reverse side if necessary and identify by block number)

Concrete	Nonlinear Systems
Constitutive Equations	Plasticity
Cyclic Loads	Viscoplasticity
Fracturing	Beam Analysis
Inelastic Action	Endochronic Theory

20. ABSTRACT (Continue on reverse side if necessary and identify by block number)

Significant aspects of plain concrete behavior under large dynamic loading were identified and used to evaluate current concrete models. Since the endochronic and viscoplastic models provide satisfactory descriptions of many significant features of concrete behavior, they were chosen for detailed study. Both models compared well with existing experimental data. To illustrate that both models were operational and that numerical analyses could be performed, a preliminary finite element analysis was performed for a beam column with a monotonically

(Over)

DD FORM 1473 1 JAN 73   EDITION OF 1 NOV 65 IS OBSOLETE

20. ABSTRACT (Continued)

increasing lateral displacement as a loading function. This fundamental work establishes the foundation for a development effort that addresses the problems of steel-concrete interaction, rate effects, and the analysis of reinforced concrete structures.

CONTENTS

Accession For

NTIS GRA&I	X
DTIC TAB	☐
Unannounced	☐
Justification	

By

Distribution/

Availability Codes

| Dist | Avail and/or Special |
| A | |

1

LIST OF ILLUSTRATIONS

LIST OF ILLUSTRATIONS (CONCLUDED)

I. INTRODUCTION

Current techniques for analyzing the dynamic response of reinforced concrete structures have not been notably successful. A possible explanation for this situation is the lack of a good constitutive model for plain concrete. The object of this study was to critically evaluate existing experimental data and constitutive models, to identify aspects of theoretical and experimental results that need improvement, and to make recommendations for future developments. In addition, one or two constitutive models that appeared promising were to be identified and these models were to be developed to the greatest extent possible over the course of the study.

This investigation showed that several models exist which are satisfactory for many conventional engineering applications. However, for structures subjected to large dynamic loads certain aspects of material behavior unique to this situation can be of greater significance. These include rate effects, cracking, nonmonotonic load paths, dilatation, and loading paths beyond the limit state, or state of maximum stress, for any point in the structure. No one model incorporates all of these effects but the endochronic and viscoplastic models do provide satisfactory descriptions of many features. Of these two theories the endochronic model appeared to be the most comprehensive and was adopted as a basis for detailed investigations. Since the model holds only for compressive states of stress, a discrete cracking model is necessary to provide a full spectrum of response capabilities.

Although a variety of plasticity models are in use, it appears that the scope of the theory has been unnecessarily restricted with the result that current models are not acceptable to the regime of interest. Thus an investigation was performed to determine if a plasticity model could be formulated that would also reflect the important response features mentioned previously.

Scatter is a fact that must be expected when evaluating experimental data. In light of the complex nature of concrete the general features displayed by published data are remarkably consistent. Although there is an

5

extensive amount of such data there are additional requirements for evaluating constitutive models in the regime of interest. One such requirement is that of response features and limit states associated with nonmonotonic loading paths. Often it is implicitly assumed that many aspects of concrete behavior are path-independent. To provide some preliminary information on this matter, a triaxial testing program was initiated at New Mexico State University (results are provided in a separate report).

Another area in which there is a surprising lack of solid data is that involving rate effects. Except for one-dimensional test results, there are no experimental data on how the stress path and limit state are affected by strain rate. Since even one-dimensional data are limited, support was provided to upgrade the INSTRON machine at the Civil Engineering Research Facility (CERF) so that uniaxial experiments could be performed on reasonably sized concrete specimens.

In summary, two constitutive models are identified, of which each has shown the capability for representing basic response features of plain concrete. An experimental program was initiated to provide new data for static behavior, and capabilities have been defined and developed to provide similar data for dynamic behavior. These data provide the basis for detailed evaluations of constitutive models. This fundamental work establishes the foundation for a development effort that addresses the problems of steel-concrete interaction, rate effects, and the analysis of reinforced concrete structures.

II. BACKGROUND

SIGNIFICANT FEATURES OF CONCRETE BEHAVIOR

Typical stress-strain curves for plain concrete subjected to uniaxial tension and compression are shown in Figure 1. In tension, concrete behaves as a nearly linear elastic-fracture material, exhibiting no significant permanent strain before it fails by the formation of a crack. A variety of schemes has been devised to handle the tensile behavior of concrete. Most of these can account for multiple cracks, cracks closing and reopening, crack shock, and residual shear resistance. Since compressive behavior is the major aspect of concrete modeling and since cracking models are, to some extent, interchangeable, the emphasis of this investigation was placed on the compressive model. In compression the initial nearly linear elastic region is succeeded by a nonlinear region at higher loads as a result of the formation of microcracks within the material. This microcracking causes permanent deformation and a loss in stiffness similar to the strain hardening seen in metals. Continued growth and intersection of these cracks decrease the stiffness of the concrete until a slope of zero is eventually reached. This point is defined as the ultimate compressive strength of the concrete (f'_c). If the load corresponding to this stress were maintained, the concrete would lose resistance and crush. However, if the concrete specimen is loaded by incrementing strain rather than stress, resistance to deformation would still be available and crushing would not immediately occur. This portion of the curve depicts the strain softening phenomenon of concrete. A similar situation would exist if the heavily loaded portion of a structural member were able to transfer part of its loading to an adjacent, less heavily loaded portion. Since load redistribution is important in inelastic behavior of materials, strain softening can be a significant feature in a concrete model.

The unload-reload cycle included in Figure 1 is somewhat idealistic, but it serves to illustrate that significant hysteresis loops can occur in plain concrete. Actual concrete behavior due to an uniaxial cyclic load is shown in Figure 2 (Ref. 1). Deterioration of the elastic modulus is indicated by the collapse of the hysteresis loops at high strain. These effects may be important in dynamic situations where considerable cycling may occur.
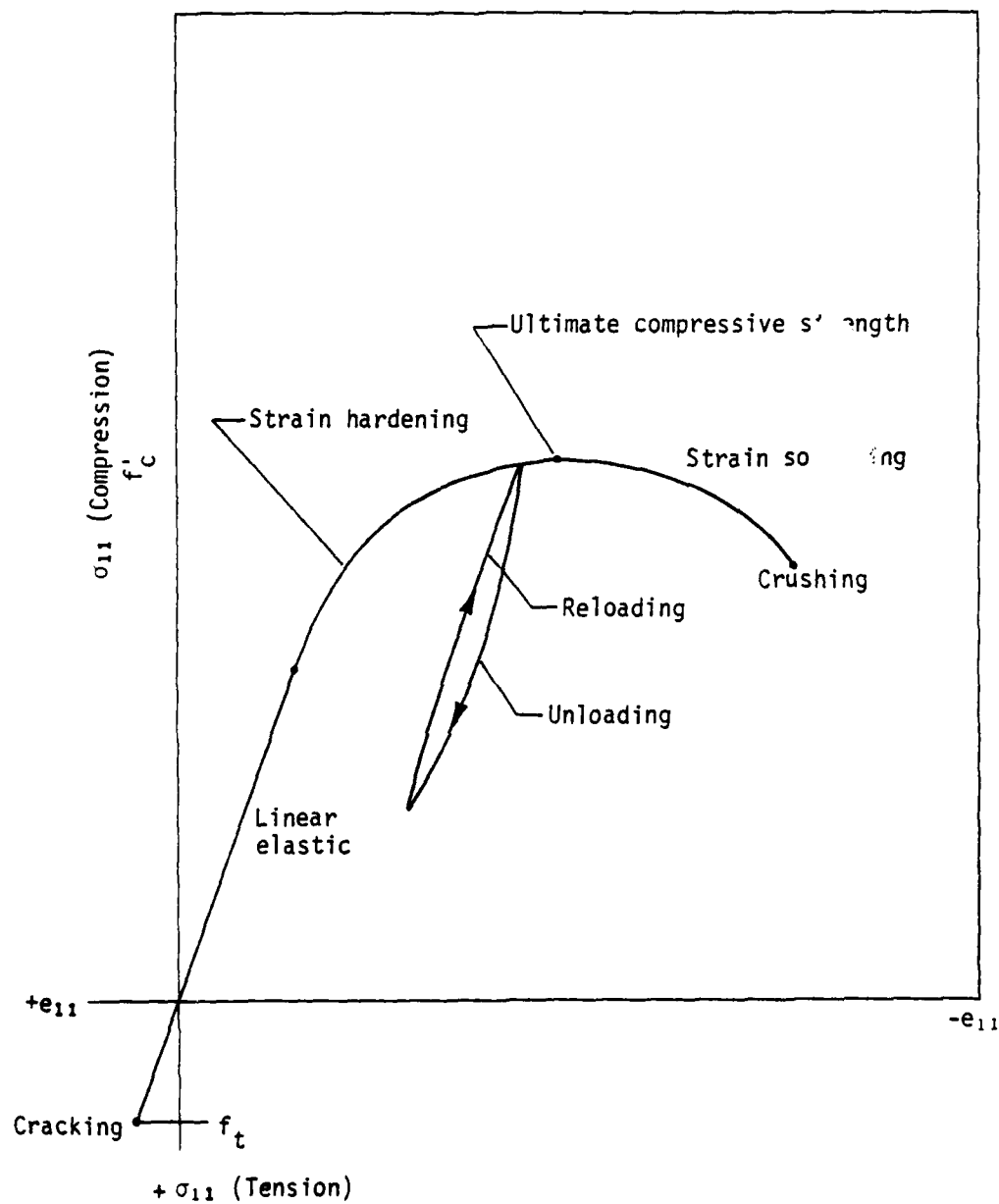
Figure 1. Typical uniaxial stress-strain relationship for plain concrete.

8
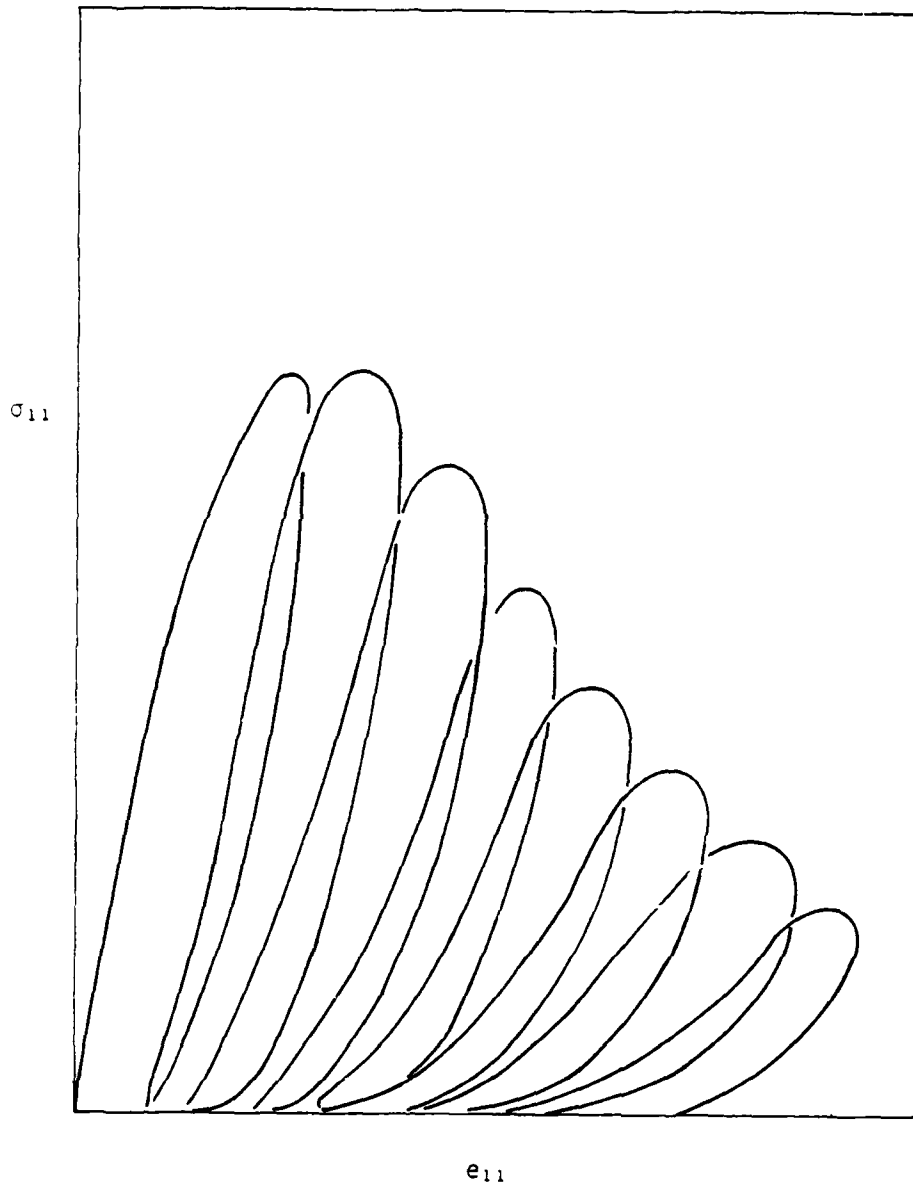
Figure 2. Behavior of cyclically loaded concrete (Ref. 1).

If a multiaxial loading is considered for plain concrete, the material behavior will be affected in the compressive state, primarily through a strengthening or weakening due to different confinement effects of the lateral stresses. The strengthening effect can be seen in Figure 3 (Ref. 2), where uniaxial and equal-biaxial loading paths are compared for a given concrete. The effect is more pronounced in Figure 4 (Ref. 3) which depicts a standard triaxial loading path consisting of uniaxial compression superimposed on a hydrostatic compressive load. It is often convenient to isolate the confinement effect by describing the loading on the concrete in invariant stress-space, where the abscissa is the first stress invariant and the ordinate is the square root of the second deviatoric stress invariant. Uniaxial and multiaxial stress states are depicted in invariant space in Figure 5. The dotted line is of interest because it represents an envelope of the failure points for the type of loading considered. It is important to note that concrete behavior is sensitive to the stress path undergone, so all failure points do not fall on the envelope. Stress path sensitivity is illustrated by the range of the failure points shown in Figure 6 (Ref. 4) for different lode angles. Although invariant stress-space is useful for depicting confinement effects, it is not sufficient for distinguishing between all possible stress paths. Such a distinction must be made by considering a plot of the stress state in stress space, as shown in Figure 7 in a three-dimensional plot or in Figure 8 as sectional views. Paths (4), (5), and (6) would be indistinguishable in invariant space. In both figures a depiction of the failure envelope is sketched in.

While inelastic volumetric behavior in metals can often be neglected, this type of behavior is significant for concrete. The hydrostat shown in Figure 9 (Ref. 3) depicts one nonlinear aspect of volumetric behavior in concrete. The strain hardening-like behavior is due to crushing of the pores in the material. The same figure superimposes volumetric aspects of concrete behavior under uniaxial and standard triaxial stress paths with the confining pressure, P_0, shown. It is seen that the combination of volumetric and deviatoric loading produces positive increments of volume change (dilatation) as the ultimate strength of the material is approached. Dilatation is caused by the tendency of shear stresses to open cracks in a microcracked, brittle material.
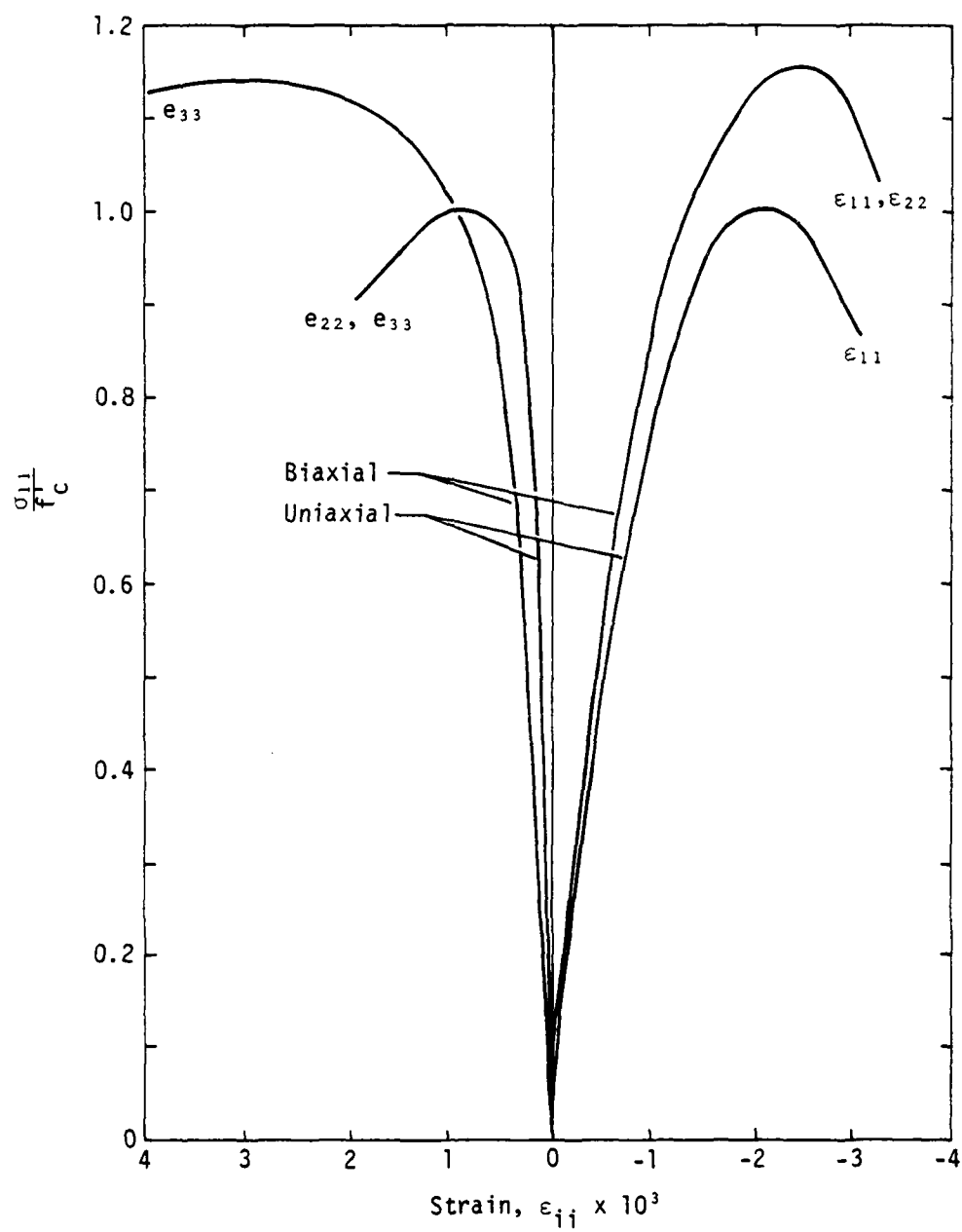
Figure 3. Comparison of uniaxial and biaxial loading paths (Ref. 2).
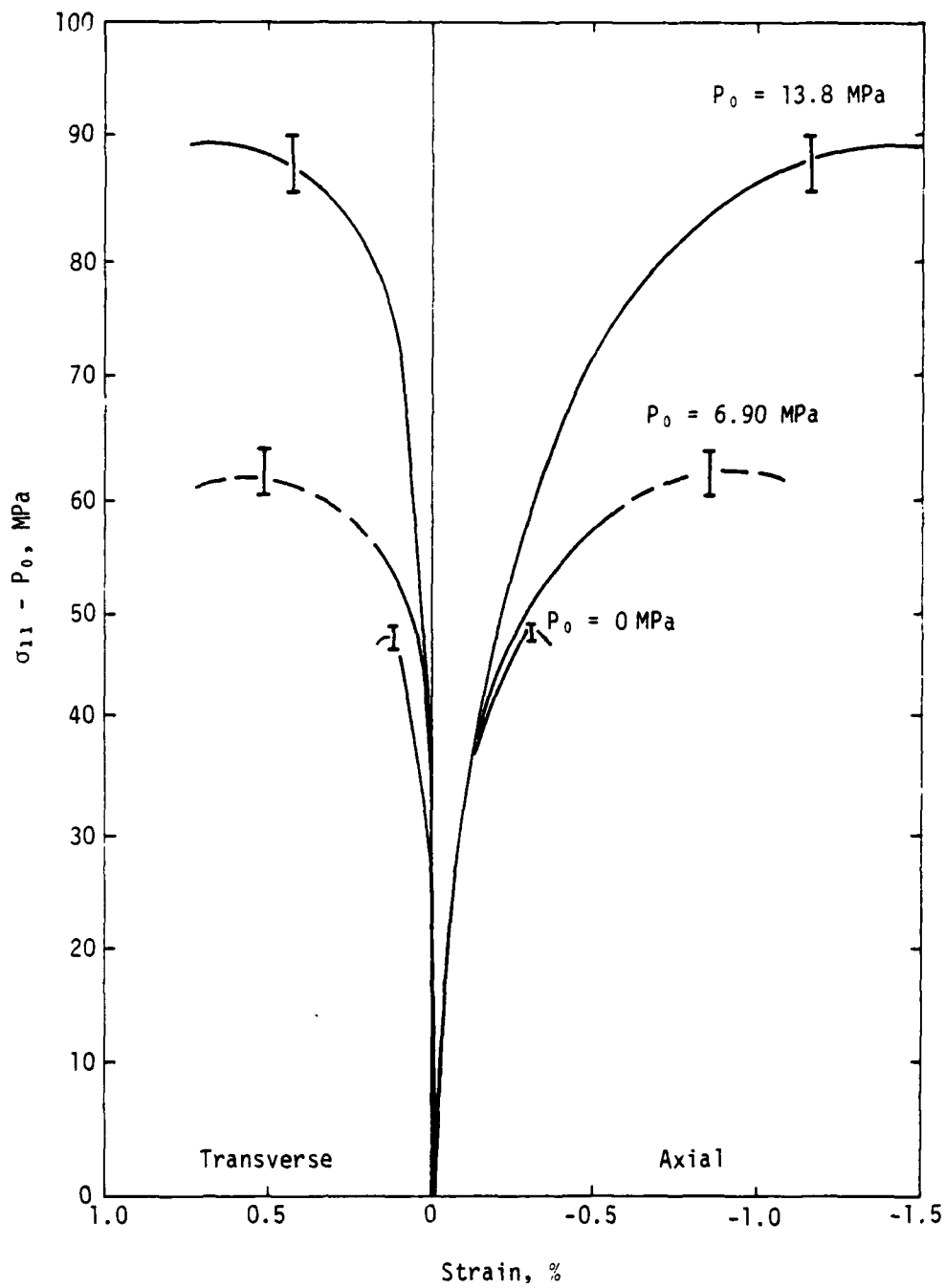
Figure 4. Principal stress-strain curves for compressive loading under constant hydrostatic **pressure**, P_0 (Ref. 3).

(1) Uniaxial stress path
(2) Biaxial stress path
(3), (4) Standard triaxial stress path

$\sqrt{J_2}$

(4)

(3)

(1)

(2)

I_1
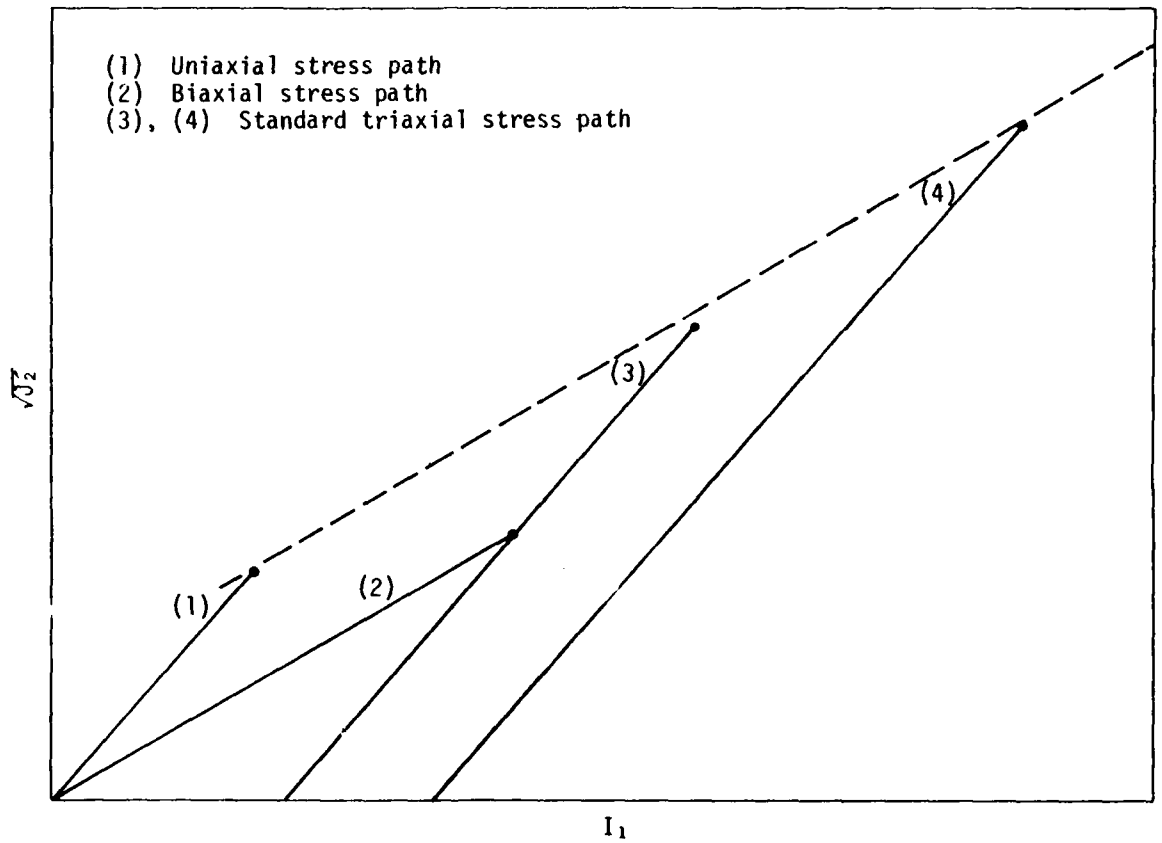
Figure 5. Concrete behavior for different loading paths shown in invariant space.
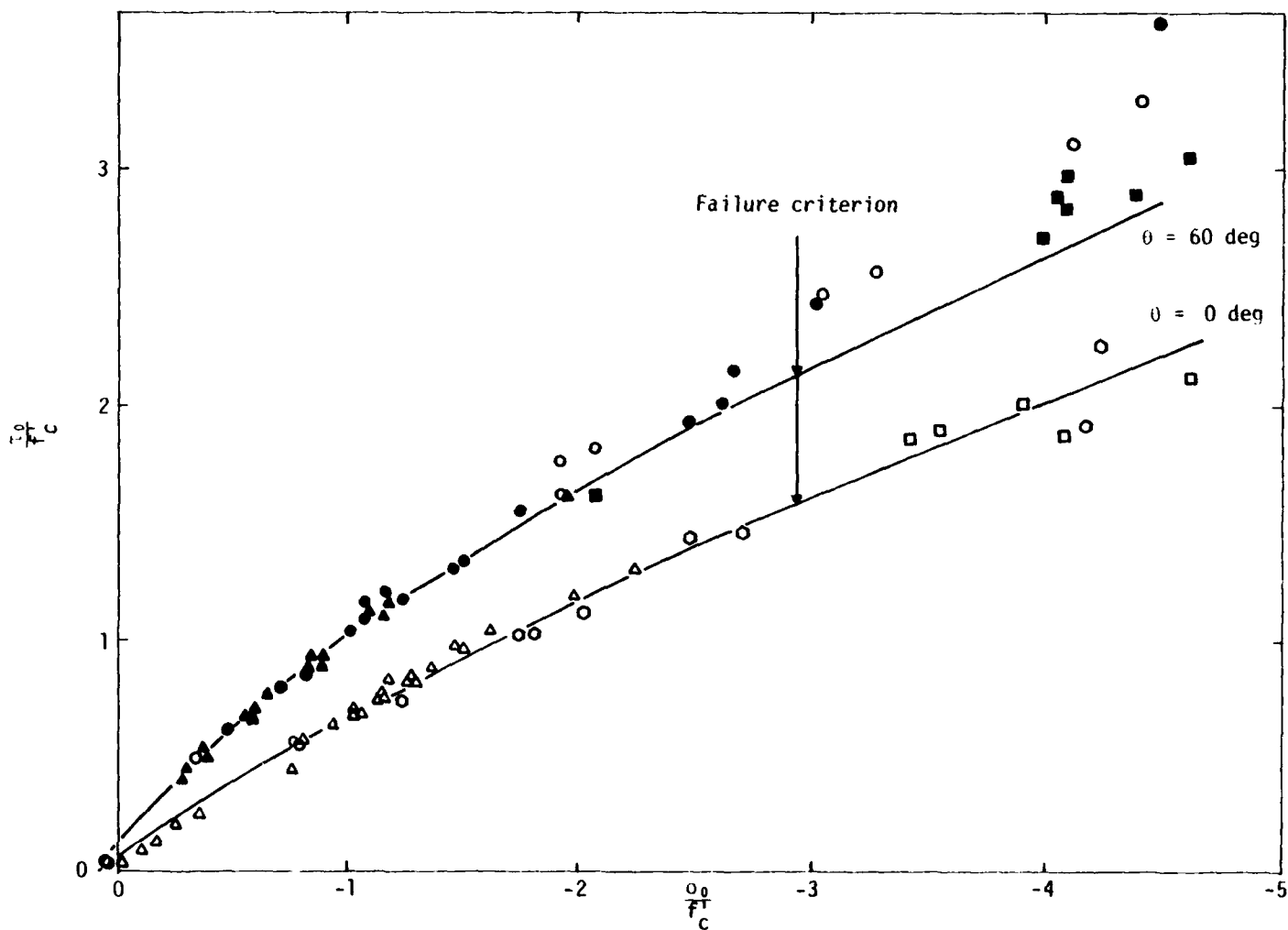
Figure 6. Effects of stress paths on failure (Ref. 4).
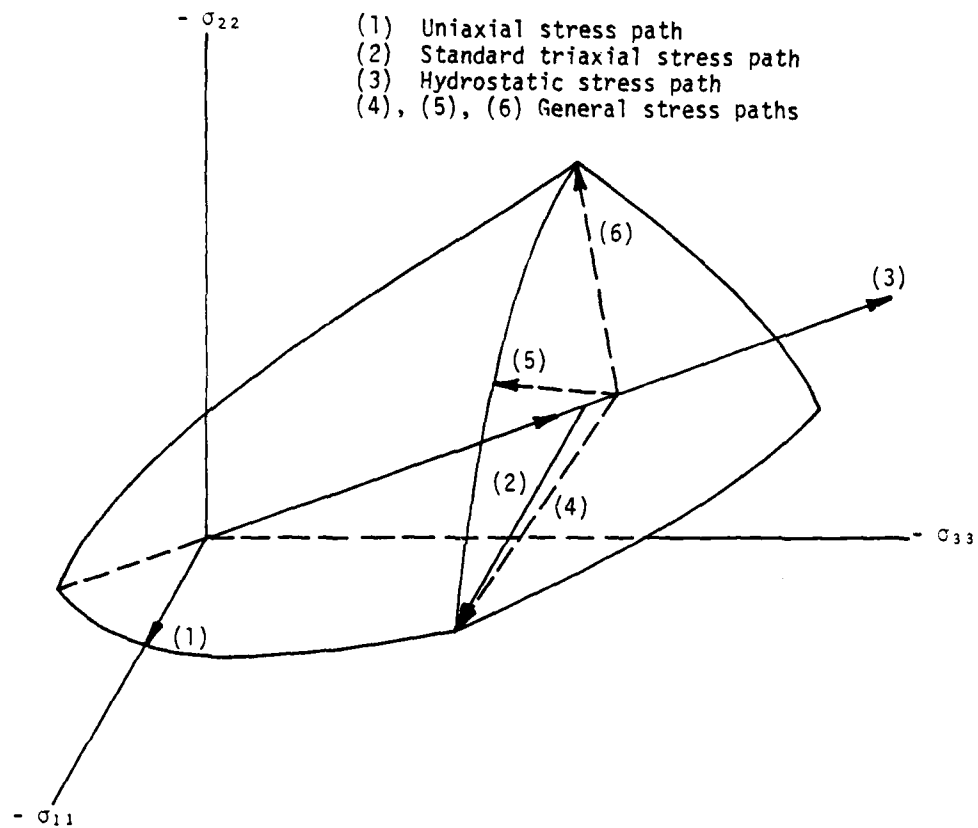
Figure 7. Stress paths in principal stress space.
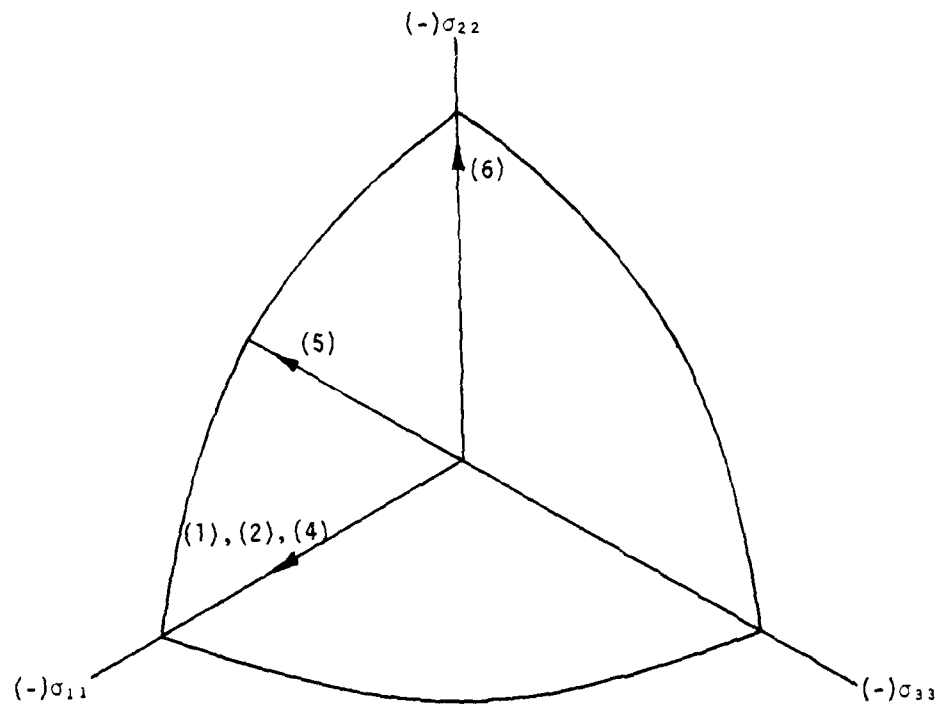
(1) Trace of uniaxial stress path
(2) Standard triaxial stress path
(4), (5), (6) General stress paths
      from Figure 7

Figure 8. Stress paths in deviatoric stress plane.

16
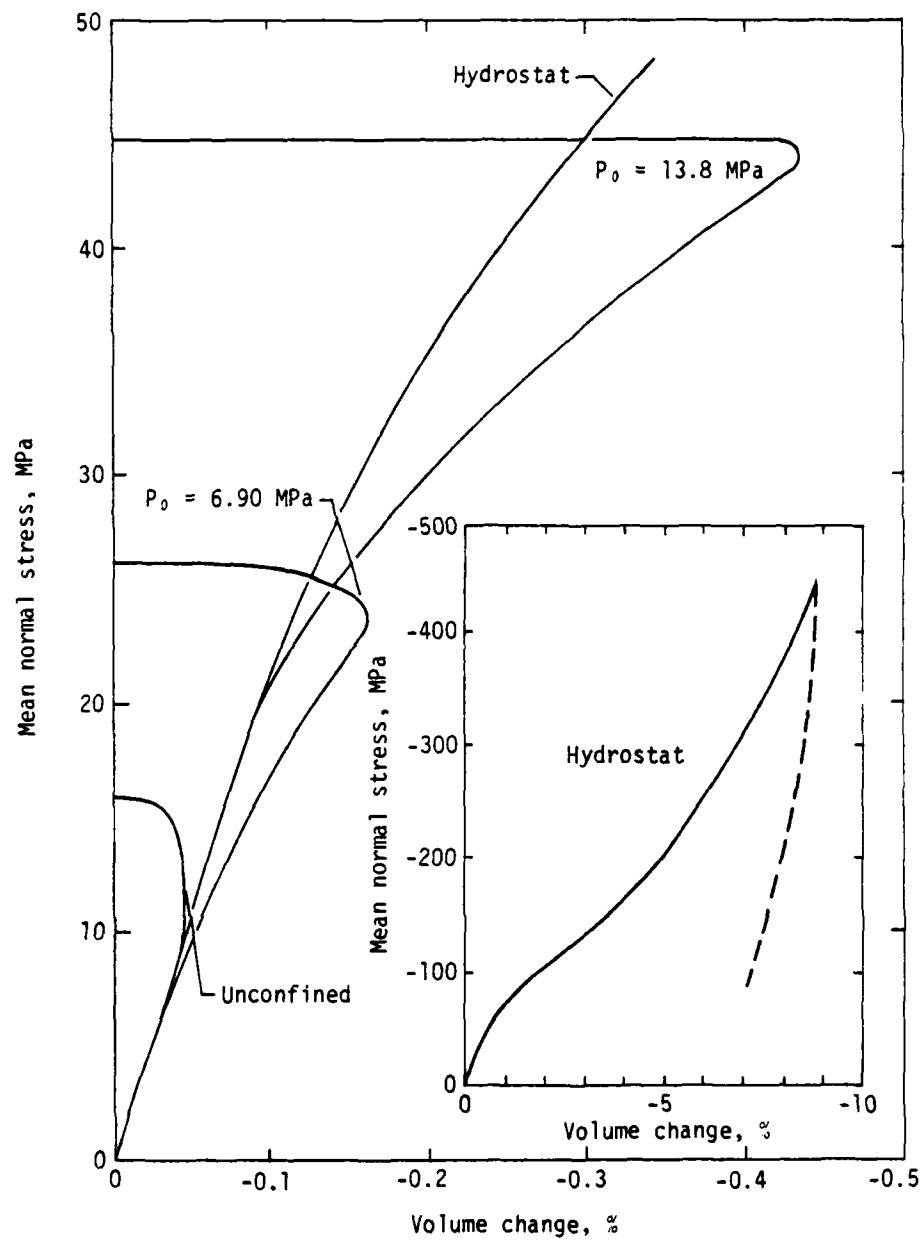
Figure 9. Volumetric stress-strain curves for constant hydrostatic
pressure tests (Ref. 3).

17

A third nonlinear volumetric effect can also be seen. This is the deviation to the right of the hydrostat which occurs for the standard triaxial stress paths and is called shear compaction.

Experimental data indicate that the unconfined (uniaxial) compressive strength and elastic modulus of concrete increase with the strain rate. This effect is illustrated in Figure 10 (Ref. 5). It must be emphasized that the accuracy of strain rate data is affected by measurement techniques and dynamic effects in the sample, loading system, and measurement system. For these reasons, existing data on strain rate effects must be viewed critically.

In summary, significant features of concrete behavior include cracking, strain hardening and softening, cyclic loading effects, confinement effects, stress path effects, volumetric inelastic effects, and strain rate effects. It may be unrealistic to expect a concrete model to duplicate all of these features and continue to be viable as a practical material model. The more likely situation would be for a user to compromise some accuracy based on what features of a material are of the most importance for the analysis involved.

CONSTITUTIVE MODELS

Plain concrete--An evaluation of a constitutive model depends to a great extent on the representation of characteristic features that are pertinent to the range of variables for which an analysis is required. Thus, for certain applications, even an elastic model is completely adequate. However, the states of importance to this study include those of strain softening and rate effects among others. Since many models were not even intended to be used in this regime, any suggestions of inadequacy must be interpreted in this light.

The plastic-fracture model in Reference 4 was developed with the complementary goals of a material model with the capability of describing the essential features of concrete behavior, yet with sufficient simplicity for ease of implementation into a finite element program. Since the model is the result of an extensive development effort, it is reviewed here in some detail. The model is based on a four-parameter criterion for a failure surface, which

18
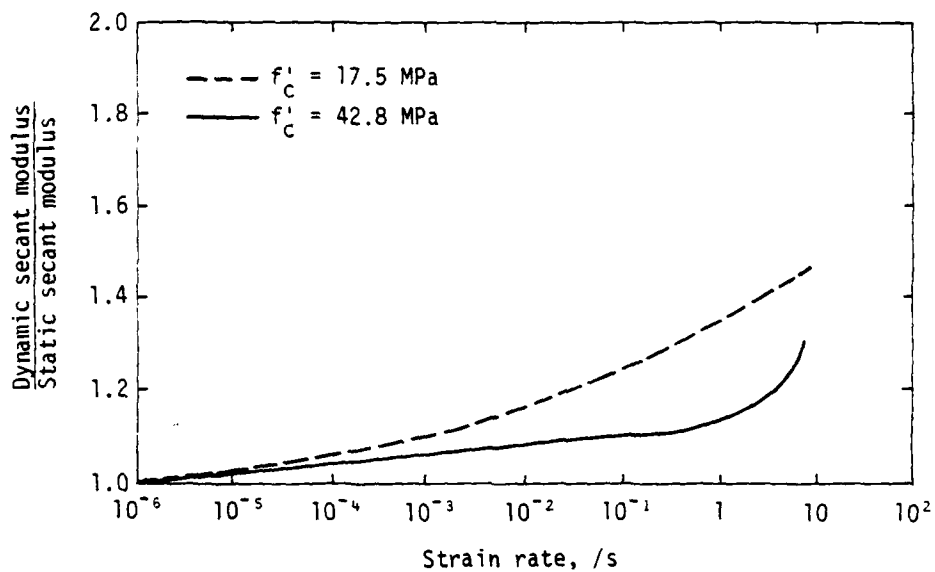
(a) Strain rate effect on secant modulus.
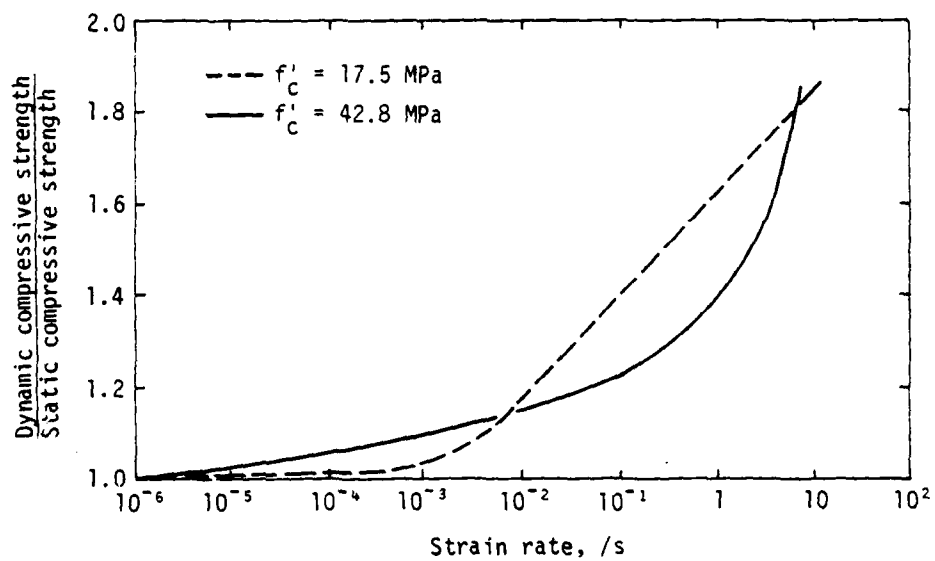
(b) Strain rate effect on compressive strength.

Figure 10. Strain rate effects (Ref. 5).

appears to match experimental data quite well. A similar but smaller surface inside the failure surface serves to define yield. Preyield and postfailure behavior is assumed elastic, while postyield-prefailure behavior is defined by an associated flow rule and Ziegler's kinematic hardening rule. A mixed hardening model is utilized. Postfailure behavior is separated into a cracking mode, a crushing mode, or a mixed mode by use of a parameter called the crushing coefficient. A cracking model which assumed anisotropic elastic postcracking behavior and allows for multiple cracking and crack closure is proposed. Parameter determination for the model can be effected with data from a uniaxial compression test.

In compression, linear elastic behavior is assumed until the yield surface is reached, and then an associated flow rule and mixed hardening rules are used to define the material behavior until the ultimate strength is reached. A consequence of the associated flow rule utilized here is a model which produces no inelastic behavior for paths tangent to the loading surface. This appears to be contrary to observed concrete behavior.

Strain softening is not built into the model, presumably for simplicity and to avoid violation of Drucker's stability postulate (Ref. 6). Instead, a simplified model of postfailure behavior which allows stress redistribution is used.

The failure surface can be depicted in the invariant plane as shown in Figure 11. The upper line corresponds to a corner of the surface, while the lower line corresponds to the center of a side. It is apparent from their shape that the associated flow rule will pick up the dilatation feature of inelastic volumetric behavior, but it cannot model the shear compaction feature. The fidelity of the resulting dilatation prediction is not indicated. At any rate, it is not known how significant this particular property is in predicting the response of indeterminate structures. Also, the open-ended nature of the surface prevents the modeling of hydrostatic inelastic volumetric behavior--i.e., pore crushing. Thus the resulting hydrostat would be linear.

20
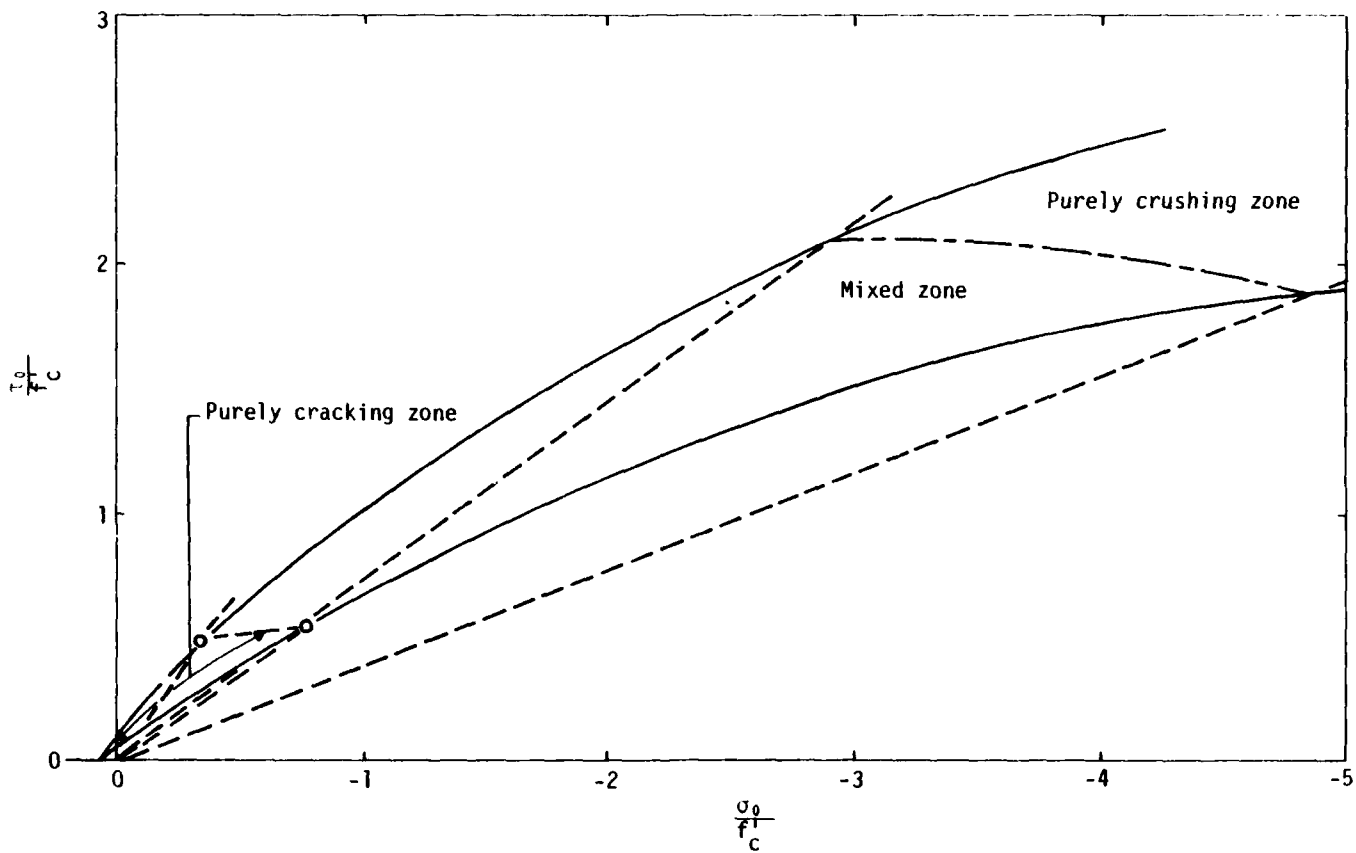
Figure 11. Failure zones in octahedral shear and normal stress plane (Ref. 4).

Postlimit behavior was apparently chosen as the area most suitable for an approximate depiction of concrete behavior. As already indicated for the uniaxial case, strain softening is not modeled per se. Postfailure behavior is described as being of the crushing type, the cracking type, or the mixed type. For pure crushing an instantaneous reduction in strength and rigidity is assumed to occur, generally to zero. On the other hand, pure cracking is assumed to result in a complete loss of rigidity on the crack face. The cracking model is sufficiently sophisticated to account for multiple cracks and cracks closing and reopening (Ref. 7). It is not apparent whether crack shock and residual shear resistance are considered. The mixed type of postfailure behavior combines a portion of the strength and rigidity reduction of the pure crushing behavior with the anisotropic aspect of the cracking behavior.

Bazant and Kim (Ref. 8) have also developed a plastic-fracturing theory in which the loading function was chosen to be of the Drucker-Prager type. The point that plastic slip does not lead to strain softening was rigorously adhered to and the mechanism of microcracking or fracturing was used to describe a decrease in stress with increasing strain. The result is a two-surface plastic-fracturing theory that matches available experimental data. However, its complexity at this stage of development appears to make it unsuitable for use in a large computer code.

Reference 9 emphasizes that the application of any plasticity theory to the analysis of concrete must be considered phenomenological since the theory is not applicable in terms of microbehavior. Whether or not such an approach is useful depends on the ability of the model to simulate macrobehavior in complex situations and the ability of the analyst to draw reliable inferences from an analysis. Here a modified plasticity theory is developed whereby the total equivalent plastic strain rate is decomposed into appropriate tensile and compressive plastic strain rates. This decomposition is based in part on the particular regime as defined, for example, in Reference 4. This provides a capability for predicting postcracking tensile response when reinforcing and prestressing are present. The approach appears to be a reasonable compromise between the representation of physical phenomena and the suitability for use in large-scale computer codes. However, the dilatational aspect of concrete in compression is not reflected in this model.

22

Dragon and Mroz (Ref. 10) formulated a brittle elastic-plastic model to describe phenomenologically the complex material behavior associated with rock and concrete. The plasticity aspect is assumed to hold for both stable and unstable portions of the stress-strain relation while a fracture parameter is coupled with irreversible volumetric dilatancy. During progressive fracture the observed phenomena of changes in elastic moduli are also incorporated in the theory. Both a yield and a fracture surface are used to provide plastic and fracture strains. Although the basic phenomena are incorporated in the formulation, the primary drawback from an analysis viewpoint is the complexity of the model. At this development stage the number of parameters that would have to be carried appears to be formidable.

Willam and Warnke (Ref. 11) have developed a theory in which a constitutive model is based on the failure criterion. A three-parameter failure surface was developed for concrete subjected to triaxial loading in the tension and low compression regime. This failure surface was subsequently modified to a five-parameter model that provides curved meridians. This nonlinear relation in the mean normal pressure provides a good fit to data into the high compression zone. These failure surfaces are used also as yield surfaces for an elastic-perfectly plastic constitutive law. As expected, the model predicts too much dilatation, a feature that is often corrected with the use of a cap (Ref. 12). In addition, elastic-perfectly brittle behavior is assumed in the tensile regime. Cracking is assumed to occur when the major principal stress reaches a limiting value and cracks are taken to be perpendicular to this principal direction.

Lade (Ref. 13) has developed a three-parameter failure surface that displays many of the same characteristics as Willam and Warnke's five-parameter model and shows a good fit with experimental data. However, this failure surface has not been related to a constitutive model for concrete although a complete formulation is available for soils (Ref. 14).

Because of the complexity of the phenomena displayed by concrete, some investigators have resorted to the development of empirical relations for stress and failure as a function of strain (Refs. 15 and 16). Although such

23

an approach is suitable for monotonic loading conditions, it only can be considered an appropriate analytical technique under a very limited set of circumstances.

The incremental relations of hypoelasticity have the inherent advantages of automatically displaying both a nonlinear response relation and a failure state. Coon and Evans (Ref. 17) specifically attempted to fit a particular set of experimental data with extremely good results. However, no attempt was made to model the postlimiting case (strain softening) or to display the dilatational features of their model. Elwi and Murray (Ref. 18) extended this approach to include functional forms that include quantities more prevalent in the concrete literature such as equivalent strain, tensile cutoff strains, and uniaxial compressive strength. Again, agreement with a limited set of data is good and the model is described with a relatively small number of parameters. In a note, Bazant (Ref. 19) claims that this model and all similar incremental formulations are not frame invariant, and, specifically, that discrepancies would appear if a loading state was specified in which the principal axes of stress or strain rotated. Elwi and Murray responded (Ref. 20) to say, in effect, that the arguments of Bazant were fallacious.

The endochronic approach to viscoplasticity has been extensively explored by Bazant and his colleagues (Refs. 21, 22, 23, and 24). Generally speaking, all significant aspects of compressive behavior except strain rate effects are reflected in the model. In particular, for a stress path that corresponds to a direction tangent to a flow surface in conventional plasticity, the endochronic model predicts a stiffness less than that based on elastic behavior. This appears to be an actual physical phenomenon that most other models do not predict.

For a full range of application in stress space, the endochronic model must be combined with a cracking model. Also, a detailed evaluation of the use of such a model for large-scale numerical analyses does not exist. Nevertheless, it is believed that this is currently the best single model for representing the variety of response features exhibited by plain concrete.

24

Reinforced concrete--In Reference 25 a limited evaluation of reinforced concrete models was performed. Cheverton's detailed evaluation included the Weidlinger Associates and Air Force Weapons Laboratory (AFWL) engineering models with the conclusion that both models grossly overestimated structural strength. The primary reason for this is that these models do not include degradation mechanisms such as concrete tensile cracking, softening in compression, and steel-concrete bond failure. It should be added that most other models suffer from similar limitations and the list could be expanded to include deterioration of elastic moduli.

Shear failure in reinforced concrete beams is a topic of considerable practical interest. A recent study (Ref. 26) illustrates, to a certain extent, the state of the art. In this study, empirical relations for concrete response, bond failure, and cracking are used in a finite element analysis of beams. Although the results are encouraging, the procedure provides very little guidance as to how more general states of stress should be handled.

Although the problem is complex, there have been some attempts to model cracked reinforced concrete. Reference 27 provides numerous theoretical and experimental references and discusses the particular problem of shear stiffness of a crack plane and its effect on the overall shear resistance of the structural element. The model includes both cyclic and monotonic behavior and can be used in the development of more general constitutive relations. Although this approach is limited to elastic behavior it does provide some insight into this difficult problem.

These studies are generally illustrative of the difficulties associated with modeling reinforced concrete. In no way do they represent all of the significant efforts that are being pursued. However, it is believed that until good postlimit models for plain concrete are obtained, it will be difficult to model reinforced concrete for the regime of interest.

REMARKS

A considerable amount of experimental data exists for providing the basis of a constitutive model. However, there are certain areas that have been generally ignored and that should be explored. They include the following:

1. unconventional loading paths including cyclic and fracture phenomena,

2. postlimit response characteristics,

3. rate effects, and

4. detailed composite behavior (reinforced concrete).

Many constitutive models for plain concrete are probably adequate for monotonic loading paths up to a limit state. However, most models do not even attempt to represent postlimit behavior, variable loading paths, or rate effects. These features must be successfully represented before there is much hope for analytically developing constitutive models for reinforced concrete.

Endochronic and plasticity theories have been extensively studied in an attempt to represent plain concrete over a wide range of state variables. Of these two, the endochronic theory appeared the most promising and consequently was chosen for additional study.

The primary reason that the plasticity approach has not been too successful is that existing formulations have excluded softening. In addition, the flow surface is often chosen to either coincide with the failure surface or to be parallel to the failure surface. Since there is no fundamental reason for these assumptions, a formulation has been proposed without these restrictions. A study was performed to determine if the basic qualitative features of plain concrete behavior could be represented. A potential advantage of this approach is that rate effects can be easily incorporated.

The next two sections summarize the current formulations for the endochronic and viscoplastic models for plain concrete.

26

III. ENDOCHRONIC MODEL

THEORY

The endochronic model of Bazant and Schieh (Ref. 22) is intended to
reproduce all significant aspects of the compressive behavior of concrete
except strain rate effects. Thus the endochronic model must be meshed with an
appropriate cracking model. Endochronic models assume that inelastic strain
accumulation can be characterized by a scalar parameter, called intrinsic
time, whose increment is a function of strain increments. In earlier work
(Refs. 7 and 8) it was shown that endochronic theory could reproduce aspects
of concrete behavior to a degree never before experienced. This model is a
refinement of the earlier work, serving to improve on the duplication of
observed features while removing theoretical inconsistencies. The primary
changes involved 1) separate consideration of inelastic strains related to
plastic slip of the microcracked material and inelastic strains related to
strength and rigidity degradation due to microcracking; 2) a more detailed
modeling of inelastic volumetric behavior; and 3) institution of a load-unload
criteria along with jump-kinematic hardening to better match hysteresis and
ensure energy dissipation under cyclic loading.

The intrinsic time parameters used in this model are defined in terms of
the deviatoric strain path, whose increment is

$$d\xi = \sqrt{\frac{1}{2} de_{km}^d de_{km}^d}$$

where

ξ is the deviatoric strain path length

and

de_{km}^d is the deviator of the strain increment tensor

A separate intrinsic time parameter is used for plastic and fracturing deviatoric inelastic strains, so that

$$de_{ij}^{d(pl)} = \frac{\overset{*d}{\sigma}_{ij}}{2G} d\zeta \tag{1}$$

and

$$de_{ij}^{d(fr)} = e_{ij}^{*d} d\kappa \tag{2}$$

where

$de_{ij}^{d(pl)}$, $de_{ij}^{d(fr)}$ are, respectively, the plastic and fracturing inelastic strain increments

G is the elastic shear modulus

$$\overset{*d}{\sigma}_{ij} = \sigma_{ij}^{d} - \alpha_{ij}$$

σ_{ij}^{d} *is the deviatoric stress*

$$e_{ij}^{*d} = e_{ij}^{d} - \alpha_{ij}'$$

e_{ij}^{d} *is the deviatoric strain*

α_{ij}, α_{ij}' are jump-kinematic hardening parameters

$d\zeta = cF_1 d\xi$ (plastic intrinsic time increment) $\tag{3}$

$d\kappa = cF_2 d\xi$ (fracture intrinsic time increment) $\tag{4}$

c is a coefficient defining the loading condition

and

F_1 and F_2 are invariant functions of stress, strain, and ξ.

28

The particular forms of F_1 and F_2 are determined empirically. Expressions similar to Equations 1 and 2 are developed for the dilatational and shear compaction aspects of inelastic volumetric behavior. However, inelastic volumetric behavior due to pore crushing is related to the volumetric strain path length rather than deviatoric strain path length. The volumetric strain path length is defined as

$$d\xi^1 = |de_{kk}|$$

The earlier endochronic model did not accurately reproduce the hysteretic behavior which occurred during unload-reload cycles and, in fact, violated Drucker's stability postulate. Rectifying these problems required the institution of loading-unloading criteria with appropriate adjustments for these situations. Separate criteria were chosen for deviatoric and volumetric behavior based, respectively, on deviatoric and volumetric work. Adjustments to unload-reload cycles are then partially made by selecting appropriate values of the constant parameter, c, in Equations 3 and 4, along with a similar parameter involved in the pore crushing contribution to the inelastic volumetric strains. In addition, jump-kinematic hardening is included to complete the unload-reload model.

The actual form of functions F_1 and F_2 in Equations 3 and 4 and of similar functions for inelastic volumetric behavior is determined by fitting data to a form arrived at from a combination of physical reasoning and experience. The resulting expressions are relatively complicated and are not unique--i.e., variations of the form and parameters in the functions could produce equally satisfactory fits to the experimental data. In this study an algorithm for the endochronic theory was developed and encoded to facilitate the investigation of the model. A slight variation of the form of function F_2 was necessary to produce a satisfactory fit to experimental data. The resulting model produced results which differed slightly from those of Reference 24.

EVALUATION

Results of the modified endochronic model are compared to experimental
results in Figures 12 through 19. Figures 12 through 14 demonstrate the abil-
ity of the model to duplicate uniaxial and biaxial compressive behavior,
including strain softening. Comparisons with experimental data for uniaxial
cyclic loading are shown in Figure 15. It is seen that the modified endo-
chronic model produces hysteresis loops and models the degradation of the
elastic modulus. Figures 16 through 18 compare the modified endochronic model
with experimental data for standard triaxial loading. Figure 18 demonstrates
that all three aspects of inelastic volumetric behavior are well-modeled.
Similar comparisons for nonstandard triaxial tests are given in Figure 19.
The modified endochronic model somewhat overpredicts the experimental data for
the nonstandard triaxial test.

Since the endochronic theory models material behavior without reference
to a yield or failure surface, an investigation was made to determine whether
some surface would be associated with the failure conditions predicted by the
modified endochronic theory and to determine what, if any, stress path effects
would be predicted by the model. Thirteen stress paths were considered for a
concrete with ultimate compressive strength (f_c^-) of $3.40 \times 10^-$ Pa (4930
lb/in^2). Loadings were defined in terms of strain increments and failure was
considered to occur at the maximum stress attained. The loading paths and
associated failure points are depicted in invariant space in Figure 20. All
paths would project onto the deviatoric plane as lines directed at $\div$ = 0, 30,
or 60 deg in Figure 21. The specific loading paths are described in Table 1.
Failure points for paths 1, 2, and 3, which all lie in the same deviatoric
plane, and for paths 6, 7, and 8, which all lie in the same deviatoric plane,
are also plotted in Figure 21.

Analysis of these data reveals two important aspects of the endochronic
model.

1. The model implies a failure surface in the deviatoric plane which is
consistent in form to that observed experimentally, as seen in Figure 21 and
indicated in Figure 20.

30
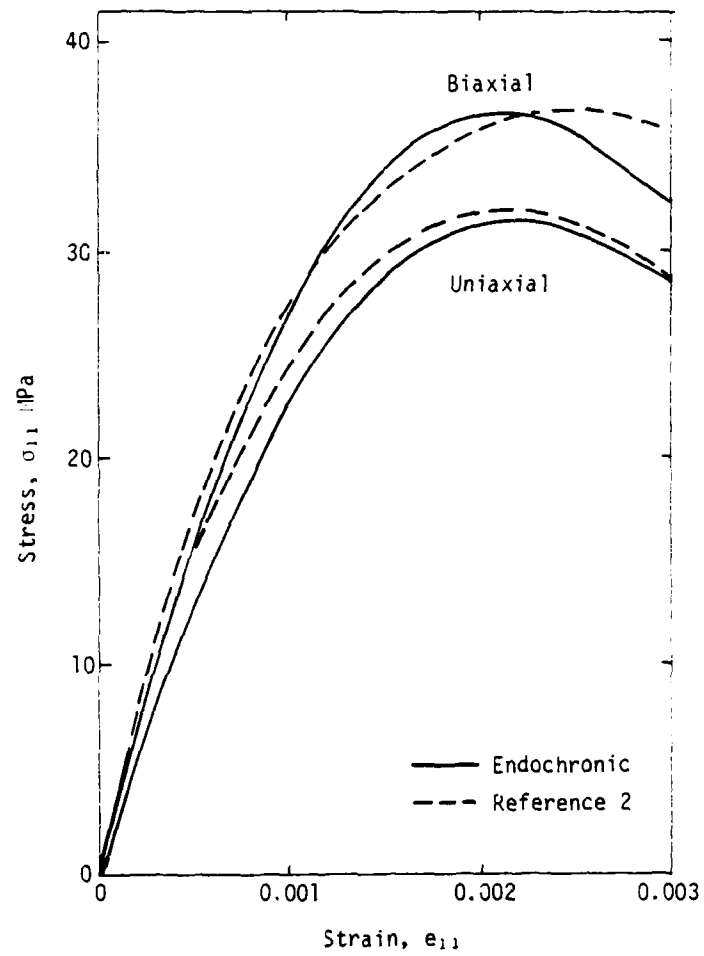
Figure 12. Stress versus strain for uniaxial and biaxial loadings.
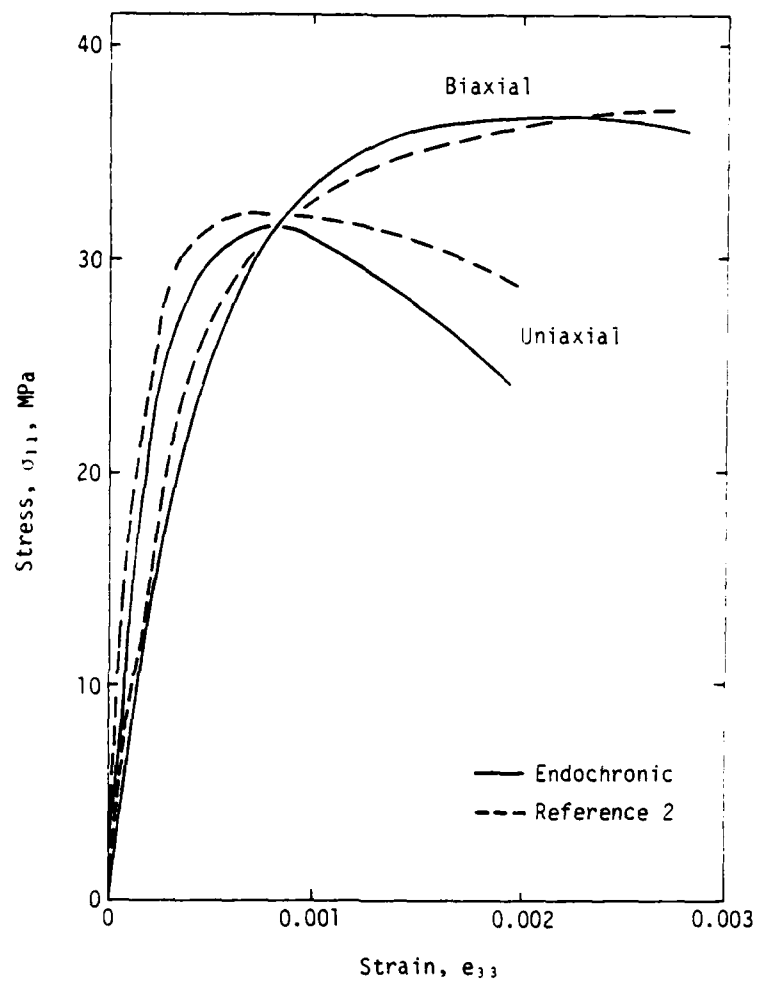
Figure 13. Stress versus transverse strain for uniaxial and biaxial loading.

32
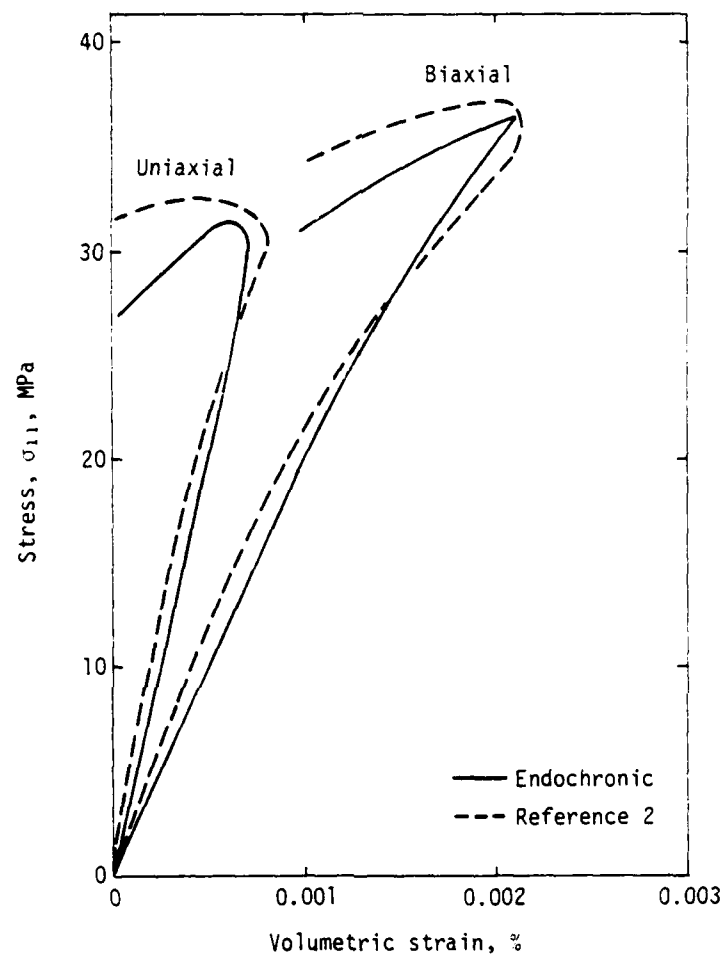
Figure 14. Stress versus volumetric strain for uniaxial and biaxial loadings.
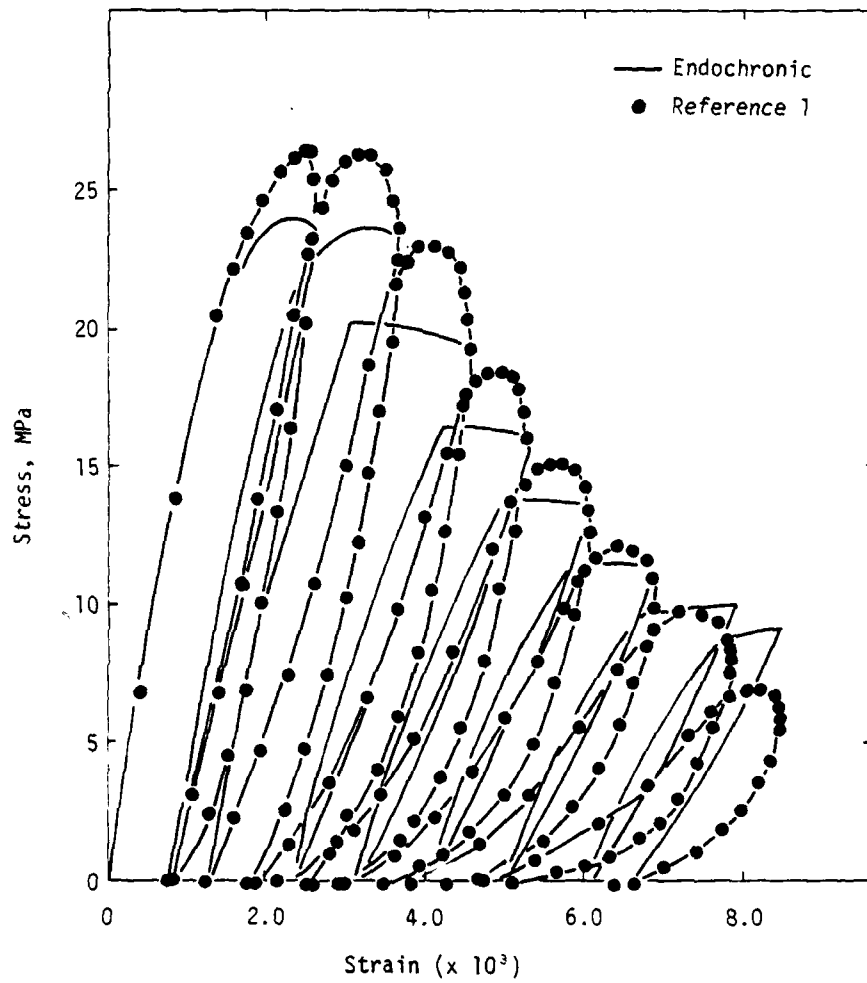
Figure 15. Stress versus strain for uniaxial cyclic compression.
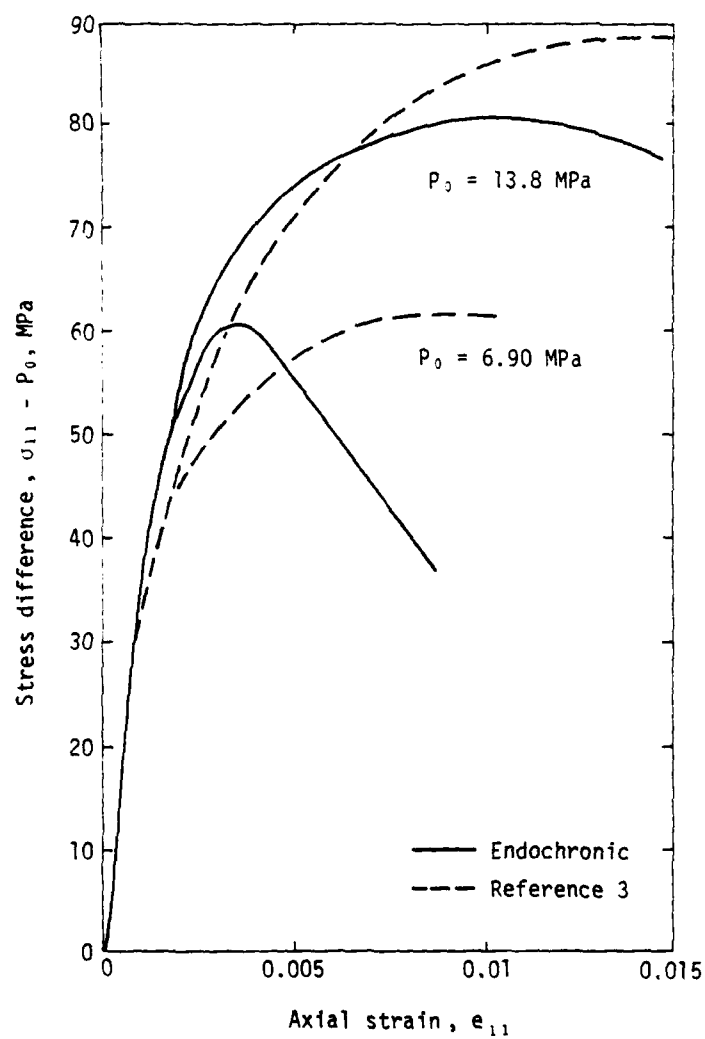
Figure 16. Stress difference versus axial strain for compressive
loading under constant hydrostatic pressure, P_0.
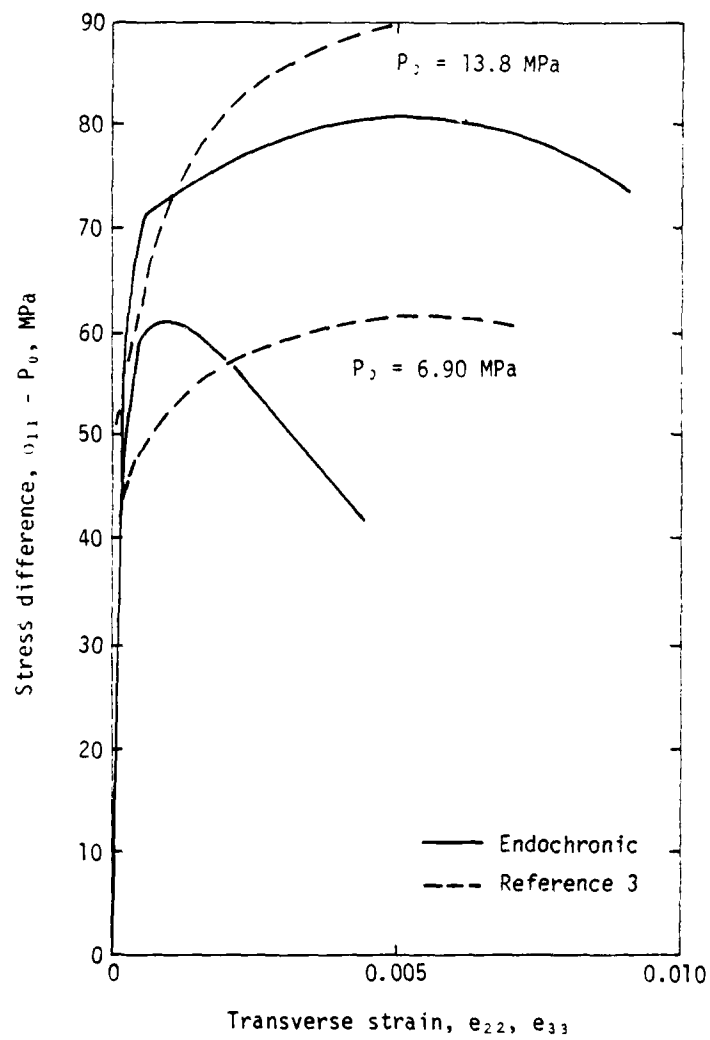
Figure 17. Stress difference versus transverse strain for compressive
loading under constant hydrostatic pressure, P_0.
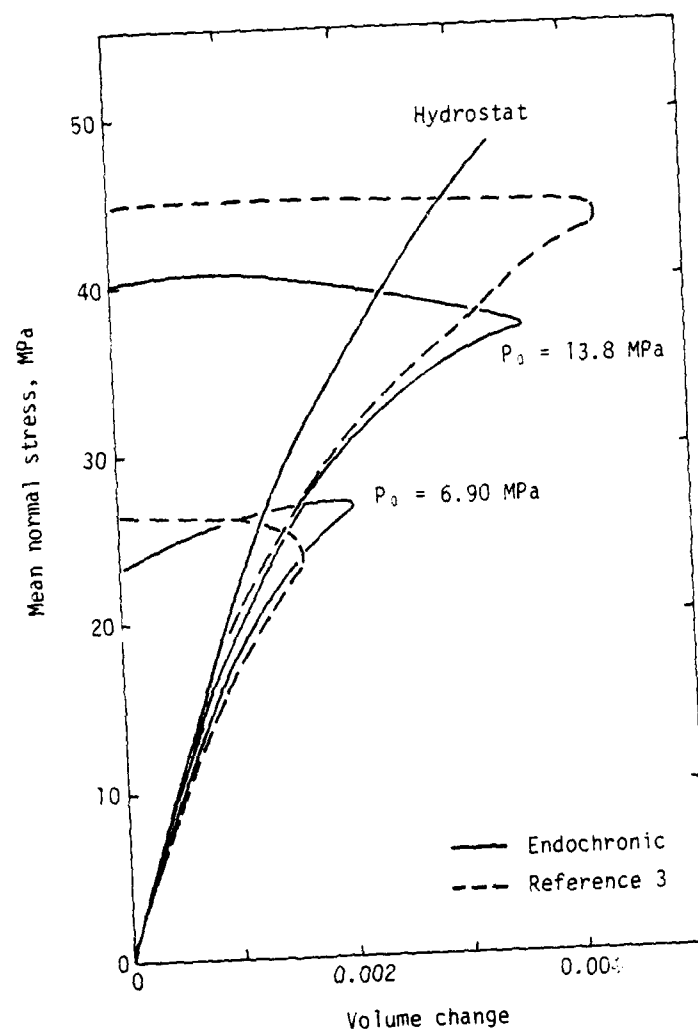
Figure 18. Volumetric stress-strain curves under constant hydrostatic pressure, P_0.
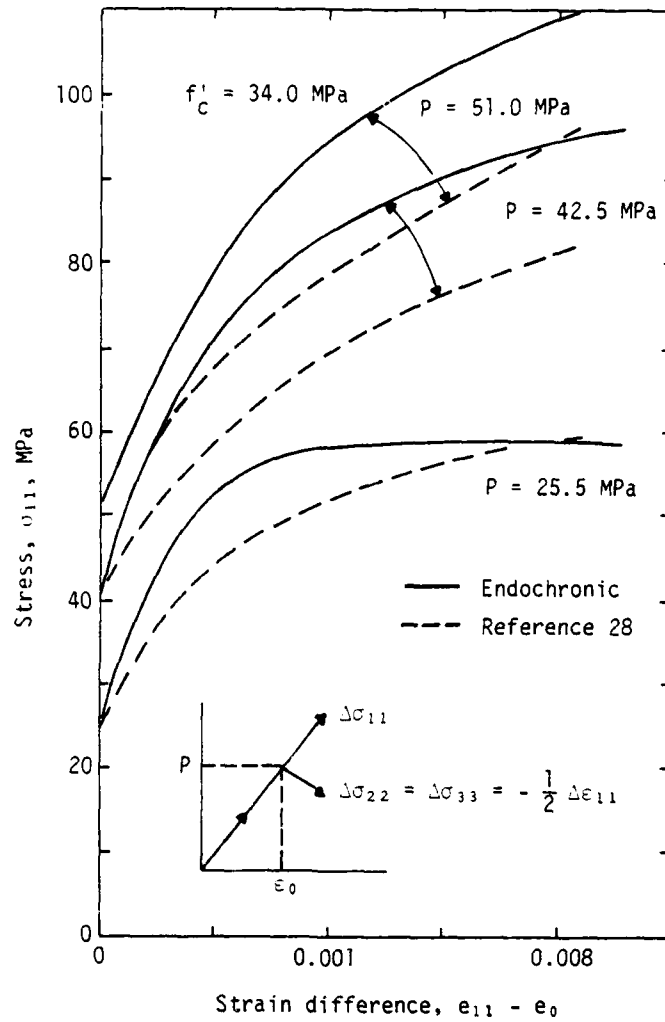
Figure 19. Stress versus strain difference for nonstandard triaxial loading.
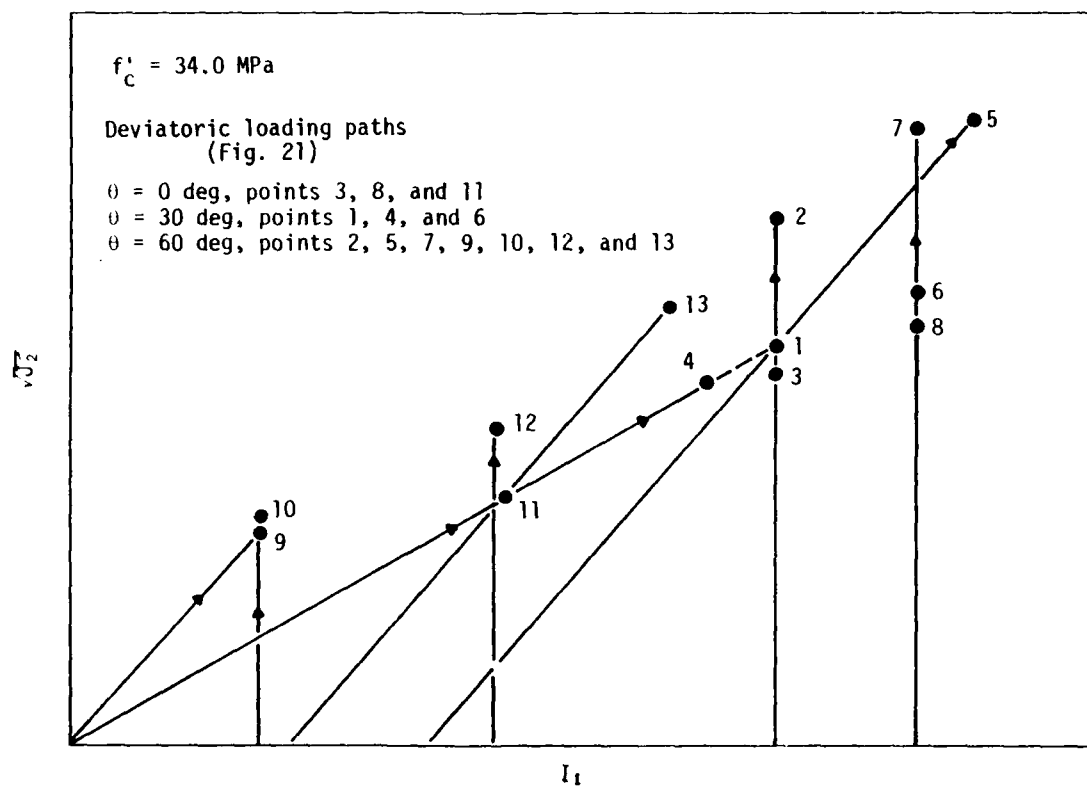
Figure 20. Failure points for different loading paths in invariant plane.
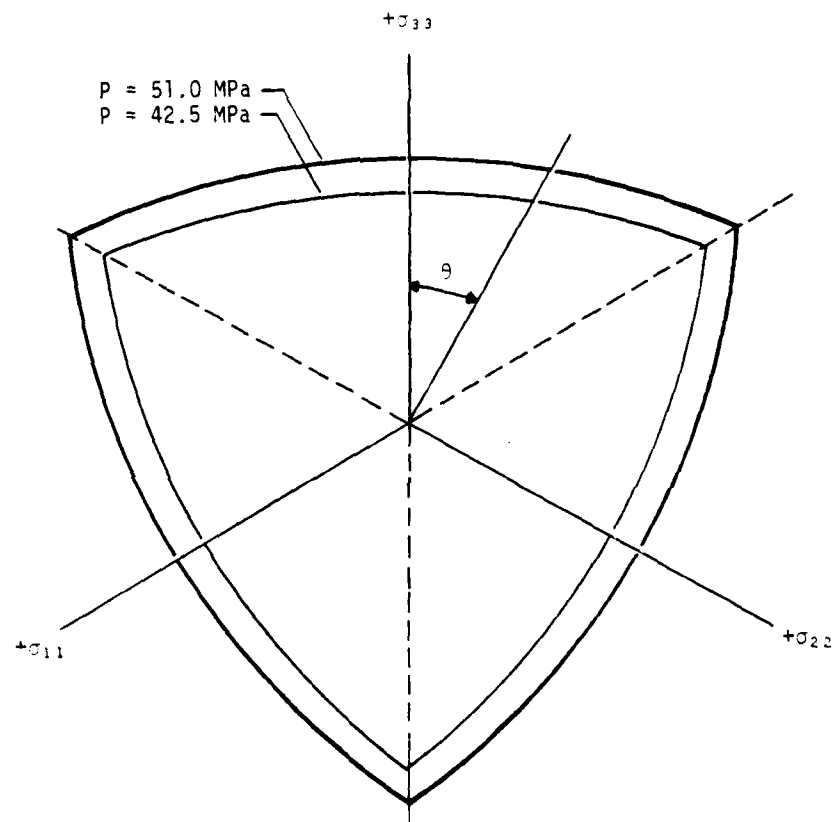
Figure 21. Failure definition of endochronic theory in deviatoric
stress plane for different mean normal pressures (P).

TABLE 1. LOADING PATHS FOR FIGURE 20

Loading path	Description
1	Hydrostatic loading to a pressure of 42.5 MPa (6160 lb/in^2); continued loading with $\Delta\sigma_2 = 0$; $\Delta\sigma_3 = -\Delta\sigma_1$ ($\sigma_{1,2,3}$ are principal stresses).
2	Same as 1 except continued loading is $\Delta\sigma_2 = \Delta\sigma_3 = -\Delta\sigma_1/2$.
3	Same as 1 except continued loading is $\Delta\sigma_2 = \Delta\sigma_1$; $\Delta\sigma_3 = -2\Delta\sigma_1$.
4	Proportional loading on path through the failure point stresses for load path 1.
5	Compressive loading under constant confining pressure through the failure point of load path 1 in the invariant plane.
6	Same as 1 except hydrostatic loading is to a pressure of 51.0 MPa (7400 lb/in^2).
7	Same as 2 except hydrostatic loading is to a pressure of 51.0 MPA (7400 lb/in^2).
8	Same as 3 except hydrostatic loading is to a pressure of 51.0 MPa (7400 lb/in^2).
9	Uniaxial loading.
10	Same as 2 except hydrostatic pressure corresponds to the mean normal stress at failure for load path 9.
11	Biaxial loading.
12	Same as 2 except the hydrostatic pressure corresponds to the mean normal stress at failure for load path 11.
13	Compressive loading under constant confining pressure through the failure point of load path 11 in the invariant plane.

41

2. The nature of the endochronic model is to produce failure dependence on the stress path, other than what would be predicted by a failure surface. This can be seen in Figure 20 for the loading paths in the 60-deg direction. The lack of a smooth curve defining failure for the 60-deg direction indicates the effect of different stress paths. Similar distinctions can be made by comparing the results of paths 9 and 10 and paths 1 and 4. Conclusive experimental data on the effect of stress path on failure are unavailable, but it could be argued that the intrinsic time serves as an approximate measure of damage accumulation during the loading process.

The monotonically increasing aspect of the intrinsic time term in endochronic theory would cause it to produce inelastic strain increments for all deviatoric strain increments, including loading tangent to what could be considered the failure surface. The resulting predicted behavior would be somewhat softer than observed concrete behavior and considerably softer than the elastic behavior predicted by a classical plasticity approach to inelastic behavior (Ref. 23). This indicates that the endochronic theory is more conservative in its depiction of loading to the side than classical plasticity approaches.

The endochronic model is one of compressive behavior of concrete, so it must be combined with an appropriate tensile/cracking model to provide a complete description of the material behavior. The tensile/cracking model is thus discrete in that it is not integrated with the compressive model. A suitable model has been devised which will account for multiple cracks, closing/reopening of cracks, crack shock, and residual shear resistance.

POTENTIAL

The Bazant-Schieh endochronic concrete model has demonstrated an ability to provide an adequate description of all significant aspects of the compressive behavior of concrete except strain rate effects. Thus features such as strain hardening and softening, cyclic loading effects, confinement effects, path effects, and volumetric inelastic effects are all accounted for. It has been demonstrated that a failure surface similar to that observed in experimental studies is produced by the endochronic model. The model demonstrates a failure dependence on the stress path other than what would be

42

predicted by a failure surface. Also, unlike models which invoke an associated flow rule, the endochronic model produces inelastic behavior for loadings tangent to what could be considered a failure surface. There is reason to believe the endochronic model is compatible with concrete behavior in this respect.

A major advantage of the endochronic model is the apparent feasibility of utilizing the intrinsic time term for the introduction of strain rate effects into the material model. Such an approach has been used to model creep in concrete and high strain rate effects in metals. The appropriate form of the intrinsic time term would have to be determined, but implementation into the material model should be a simple task.

Adjustment of the endochronic model to most concretes can be done by inputting the appropriate standard compressive cylinder test strength, f_c'. If a satisfactory representation of the material behavior does not result, two alternate adjustment methods are suggested. The first method involves using an equivalent cylinder strength in the model which provides a better analytical match to uniaxial test data than the actual cylinder strength. The second method requires adjusting the parameters of the model through a curve fit to data from a variety of tests.

The endochronic model formulation is three dimensional, although the algorithm used in this study is two dimensional. A complete triaxial algorithm would be complicated primarily by the complexity of a three-dimensional cracking formulation, which is essentially independent of the endochronic (compressive) model.

The overall efficiency of the endochronic model remains to be studied. Although the algorithm for the model is not particularly large, the storage requirement for each element appears to be somewhat larger than for other concrete models. Since the model is not incrementally linear, an iteration loop is necessary within the model, causing a slight increase in computer time.

IV. VISCOPLASTIC MODEL

THEORY

Plasticity is normally associated with the rate-independent part of the inelastic deformation of metals. The physical motivation for such a theory in that context is well-founded and plasticity is now a classical subject in the mechanics of deformable media.

Since the theory has such a well-developed mathematical basis, it is proposed to use the approach to describe the behavior of concrete as well as metals. However, here the physical insight is not as profound so a judgement on the utility of such a model must be based on the ease of application and the degree to which experimentally observed phenomena can be predicted. Furthermore, since the regime of interest includes strain rates of the order of 1/s, rate effects are important and are included by an extension of the theory of plasticity to viscoplasticity.

Frequently plasticity is interpreted to mean inelastic deformation with no increase in stress, i.e., no strain hardening. The formulation for modeling concrete must admit both hardening and softening with respect to strain and other parameters even though Drucker's stability postulate may be violated. This is done in an attempt to describe physical phenomena with a well-established theory but for a regime beyond conventional concepts.

Let $\underset{\sim}{\sigma}$ and $\underset{\sim}{\sigma}^d$ denote the Cauchy stress tensor and the stress deviator tensor, respectively, so that

$$\underset{\sim}{\sigma}^d = \underset{\sim}{\sigma} + P\underset{\sim}{I} \tag{5}$$

where

$$P = -\frac{1}{3} \operatorname{tr}\underset{\sim}{\sigma} \tag{6}$$

The identity tensor is represented with $\underset{\sim}{I}$, the invariant P is called the mean confinement pressure, and tr denotes the trace operator. Other invariants

45

that are frequently used are the equivalent shear stress, $\bar{\tau}_s$ (or the second invariant J_2')

$$\bar{\tau}_s = \sqrt{J_2'} = \left[\frac{1}{2} tr \, \sigma^d \sigma^d \right]^{1/2}$$ (7)

and the effective stress

$$\bar{\sigma} = \sqrt{3} \, \bar{\tau}_s$$ (8)

For pure shear with $\sigma_{12} \neq 0$, it can be shown that $\bar{\tau}_s = |\sigma_{12}|$, and for uniaxial stress with $\sigma_{11} \neq 0$, $\bar{\sigma} = \sigma_{11}$.

It is assumed that strains are sufficiently small (less than 20 percent) so that the total strain, e, can be considered the sum of elastic, e^e, and inelastic, e^i, parts:

$$e = e^e + e^i$$ (9)

Following the classical approach, suppose that the boundary between elastic and inelastic behavior is defined by a relationship involving stress and strain which is given symbolically by

$$\phi \left(\sigma, \, e^i, \, \dot{e}^i_j \right) = 0$$ (10)

with purely elastic behavior defined by $\phi < 0$. A superposed dot denotes differentiation with respect to time. If Drucker's stability postulate is invoked then $\phi = 0$ represents a convex surface in stress space and the inelastic strain increments are given by an associated flow law

$$de^i = g \, d\phi$$

$$g = \frac{\partial \phi}{\partial \sigma}$$ (11)

46

for a monotonically increasing scalar function, λ. To obtain the stress tensor for a load path defined by the total strain, these relations must be combined with the elastic constitutive relation

$$\sigma = C\, e^e \tag{12}$$

where C is the elasticity tensor.

Many computer codes designed for the analysis of dynamic problems utilize direct time integration. This implies that when a call is made to a constitutive equation algorithm, new values of total strain are available and that the increments in strain are small. Thus, with a counter initiated at $N = 1$, an iteration procedure for obtaining stress is given as follows:

1. Assume the increment is elastic and use current values of total strain and previous values for components of the inelastic strain tensor.

$$\sigma_N = C\left(e - e^i_{N-1}\right) \tag{13}$$

2. Evaluate the flow function.

$$\phi_N = \phi\left(\sigma_N,\ e^i_{N-1},\ \dot{e}^i_{N-1}\right) \tag{14}$$

On the first step, if $\phi_1 \leq 0$, the increment was indeed elastic and the procedure is terminated. On the second or subsequent steps, the procedure is terminated if the flow condition is satisfied, i.e., $|\phi_N| < \varepsilon$ for a small positive number, ε.

3. Evaluate components of the inelastic strain and strain rate tensors in terms of a scalar increment, $\Delta\lambda_N$.

$$e^i_N = e^i_{N-1} + \Delta\lambda_N \frac{\partial\phi}{\partial\sigma}$$

$$\dot{e}^i_N = \frac{\left(e^i_N - e^i_0\right)}{\Delta t} \tag{15}$$

47

4. Solve the consistency condition for $\Delta\lambda_N$.

$$\phi\left(\xi_N,\ e_N^i,\ \dot{e}_N^i\right) = 0 \qquad (16)$$

An approximate solution is given by the first step of the Newton-Raphson procedure

$$\Delta\lambda_N = -\left(\frac{\phi}{\phi'}\right)_N \qquad (17)$$

in which ϕ' denotes the derivative of ϕ with respect to $\Delta\lambda_N$. Return to step 1.

This algorithm is a procedure for solving the set of nonlinear constitutive equations. If the strain increment is large, it is possible that the procedure will not converge to a solution. If convergence does occur, the parameter $\Delta\lambda_N$ will be progressively smaller, so in a certain sense the procedure is self-adaptive, i.e., the step size as reflected by the value for $\Delta\lambda_N$ adjusts automatically to the degree of inelasticity with ϕ as the measure.

For most metals, inelastic deformation can be considered independent of the mean pressure, but this is not the case for concrete. Guided by observations made on experimental data for triaxial loading paths, it is postulated that in stress space a reasonable form of the flow function and its associated derivative are

$$\phi = \frac{(P - C)^2}{a^2} + \frac{\bar{\sigma}^2}{b^2} - 1$$

$$\qquad (18)$$

$$g = \frac{2}{3}\frac{(P - C)}{a^2}\,I + \frac{3\sigma^d}{b^2}$$

As shown in Figure 22, the coordinates of the horizontal tangent point of the ellipse (point d) are (C, b). If b is considered the minor axis of the ellipse, then the major axis is denoted by a. The intercept coordinates of the ellipse with the horizontal axis are given as A and B for the left and
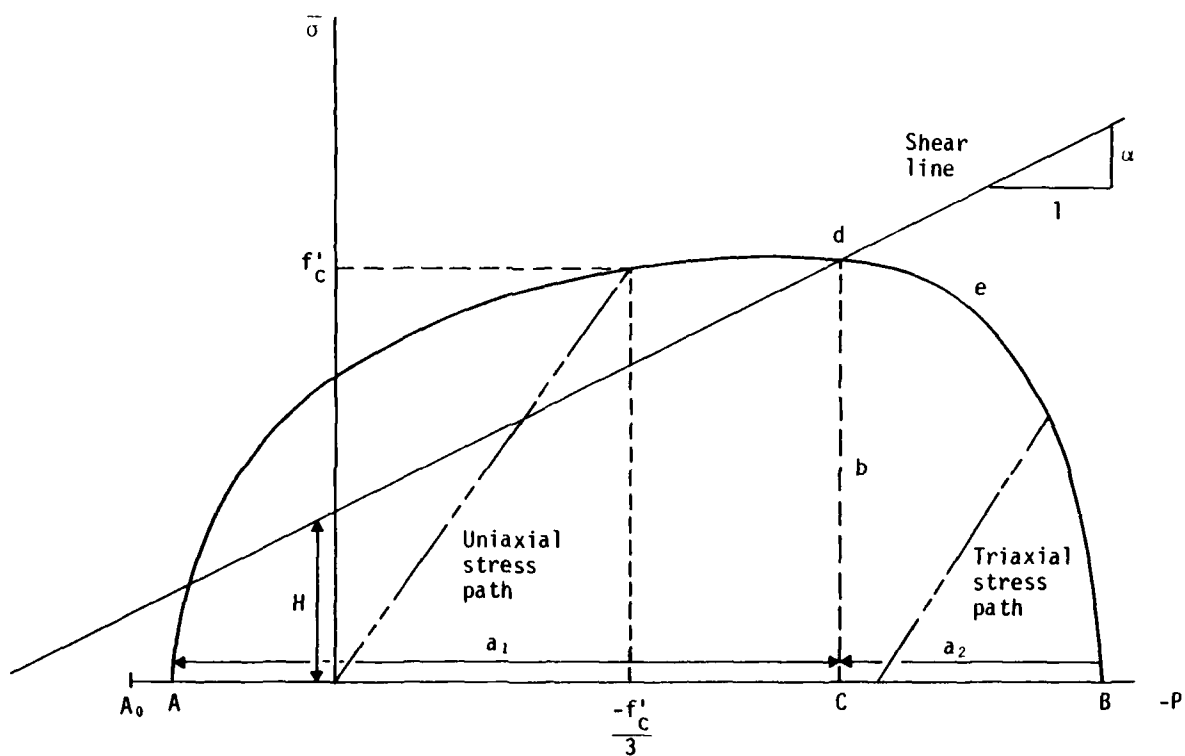
Figure 22. Form of flow surface.

right points respectively. A regular ellipse was found to be too restrictive so two major axes were defined: $a = a_1$ for $P > C$ and $a = a_2$ for $P < C$. Thus the flow surface actually consists of two ellipses with a common horizontal tangent.

Since the unit normal to the flow surface at point d is perpendicular to the P-axis, this point is associated with pure inelastic shear deformation or no inelastic volume change. Thus the locus of this point as the flow surface expands or contracts may be called a shear line. It is assumed that this line is straight with slope γ and an intercept value H on the $\bar{\tau}$-axis.

Consider the uniaxial stress compression path shown in Figure 22. Since such a loading always yields dilatation in concrete, this implies that the load point on the flow surface is always to the left of point d. At failure $\bar{\tau} = f'_c$ and $P = -f'_c/3$. Numerical trial and error calculations indicate that $\gamma = 1.0$ and at failure $C = f'_c/2$ which is a reasonable initial value. Thus a calculation based on the geometry shown in Figure 22 also yields an initial value for H of $f'_c/2$.

If $H = 0$, the model displays no strength in shear for zero mean pressure. Thus it is postulated that an isotropic failure criterion in shear can be obtained by specifying H as a function of a suitable damage function. An appropriate measure of damage may be an inelastic strain deviator defined by

$$\bar{e}^* = \int f(P)d\bar{e}^i$$

$$d\bar{e}^i = \left[tr \frac{2}{3} de^{id} de^{id} \right]^{1/2} \tag{19}$$

where de^{id} denotes the deviatoric part of the inelastic strain tensor and $f(P)$ is a weighting function chosen to reflect the fact that it is much harder to accumulate shear damage for large mean confining pressures. Until more detailed information becomes available, it is assumed that the functions f and H may be given by the simple relations shown in Figure 23.
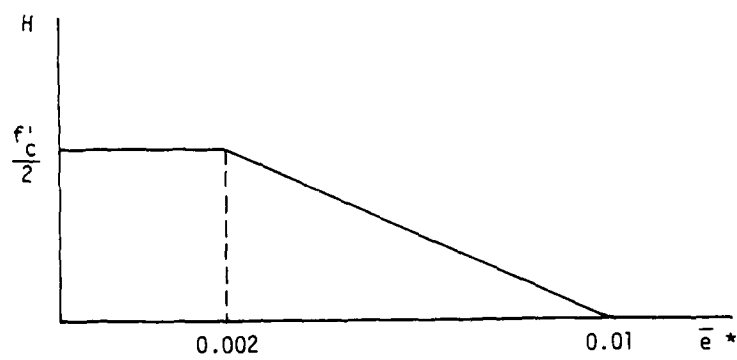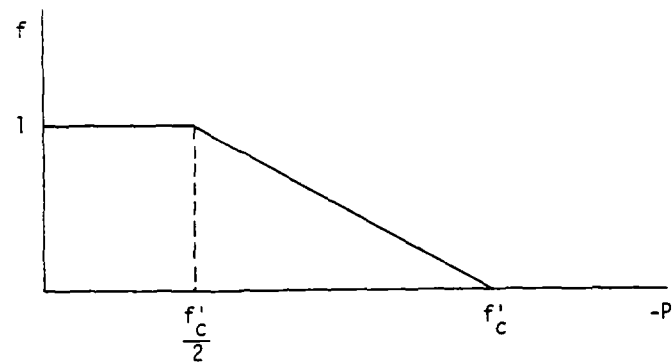
Figure 23. Assumed form of damage functions.

Under hydrostatic tension, strength of concrete is limited by tensile fracture. To reflect this, a tensile limiting value A_0 is assumed to depend on an inelastic dilatation damage function. If an increment in inelastic volume change is denoted by de_v^i, then it is assumed that

$$dA_0 = - g(P) \, de_v^i \tag{20}$$

where $g(P) = 0$ if $de_v^i < 0$ or $P < 2/3 \, f_c'$; otherwise $g = (P + 2/3 \, f_c')A_0/f_c'$ where the factor 2/3 has been chosen based on a preliminary numerical investigation.

Since the shear carrying capacity of the material may also be reduced if tensile damage occurs, it is believed to be appropriate to introduce additional shear damage according to the relation

$$(de^{-i})_T = - \bar{e}^* \, \frac{dA_0}{A_0} \geq 0 \tag{21}$$

Then, a uniaxial stress path in tension will produce both tensile and shear damage with the possibility of both A_0 and H approaching zero. Uniaxial compression produces some tensile damage since there is significant dilatation, but for other general triaxial loading paths this kind of tensile damage is limited by the fact that g is zero for large confinement stresses.

The motion of the ellipse in stress space is governed by evolution functions for the coordinates A, B, and C. Loading along the P-axis should provide a typical hydrostatic response. This is provided by assuming that an increment in the value of C is proportional to an increment in inelastic volume. In addition, under pure shear there is a tendency to evolve into a dilatational mode which means the ellipse must move to the right as the effective inelastic shear strain is increased. Both of these conditions are reflected in the equation

$$dC = \alpha_s de_v^i - \beta \, d\bar{e}^i \tag{22}$$

52

where λ_s represents a secant modulus that decreases with confinement stress

$$\lambda_s = \lambda\left(1 + \frac{P}{2f'_c}\right) \tag{23}$$

and λ denotes an initial inelastic modulus. For large confinement stress, this modulus should increase so the equation is limited to $|P| < f'_c$.

When a deformation involves inelastic volumetric strain, the effect of inelastic shear is to enhance this strain for a given mean pressure. In other words, the material appears to soften in the presence of shear. This is referred to as shear enhanced compaction for negative increments of volumetric strain and as dilatation for positive increments. This feature is reflected in the model by an adjustment of the translation feature of the ellipse. For example, for a stress state corresponding to a point on the right side of the ellipse, the volumetric, inelastic strain increment will be negative and the ellipse will move to the right. If this motion of the ellipse is decreased, the result is that the material will appear softer, which is the desired characteristic. A similar argument holds for a stress point appearing on the left side of the ellipse.

This general feature can be reflected through the sign of the function β that appears in Equation 22. For the right side of the ellipse β should be positive. The transition point for the change in sign should be to the right of $P = C$ since experimental data seem to support the onset of dilatation shortly before attaining a stress state corresponding to the horizontal tangent. The transition point, e, was chosen to be $P = C - 2/3\, f'_c$ and after some experimental investigation the following functional form was adopted for β:

$$\beta = \lambda_s \eta_2 \tanh(\eta_1) \tag{24}$$

where

$$\eta_1 = \frac{P - C + \frac{2}{3} f'_c}{\frac{2}{3} f'_c}$$

$$\eta_2 = 1 \text{ for } \eta_1 > 0 \tag{25}$$

$$\eta_2 = 1.75 \text{ for } \eta_1 \leq 0$$

With updated values of C determined by the use of Equation 22, the value
for B is obtained from

$$B = C - 2f_c'$$ (26)

For a straight shear line

$$b = H - C;$$ (27)

and the flow surface is defined once A is determined. To provide some hyster-
esis behavior, A is also allowed to vary but the purely kinematic concept of
letting A move as much as B does not appear to be justified. For convenience
a constant proportion in increments has been assumed:

$$dA = 0.15 \, dC$$ (28)

However, the tensile failure condition precludes allowing A to move further to
the left than A_o. Thus, as A approaches A_o, the increments in A are reduced
in a gradual manner so that when $A = A_o$, the increment in A is zero if $dC > 0$.

To illustrate how the model operates, consider a triaxial load consisting
of uniaxial stress superposed on a hydrostatic state of stress. Initially,
when the flow surface is first reached, compaction is enhanced over that
observed for purely hydrostatic behavior. The model reflects this feature if
the stress point falls to the right of the transition point, e, in Figure 22.
Regular volumetric strain hardening is obtained when the ellipse moves to the
right according to an inelastic volumetric strain relation. Enhanced compac-
tion is reflected by having the ellipse move to the right at a reduced rate
according to a measure of inelastic shear strain. This is reflected in the
evolution relation for C given by Equations 22 to 25.

As the ellipse moves to the right, the stress state approaches point e in
which case the enhancement effect is zero. Between points e and d inelastic
volumetric strain causes the ellipse to move to the right while inelastic
shear causes motion to the left. When the stress state lies to the left of
point d, dilatation occurs and this feature has the effect of enhancing volu-
metric expansion. By balancing these effects in the model, the stress state

54

can be held fixed, which is a situation that is observed in experiments. However, failure occurs ultimately and this is currently modeled by having the ellipse move slowly to the right under these conditions. An alternate approach might be to have the value of , decrease according to a damage function that depends on the dilatation.

Several general comments are in order. First, the hydrostatic behavior is approximated by a secant modulus that varies with the confinement stress. Rather complete analytic expressions for purely hydrostatic response are available and this could be incorporated into the theory. Second, for the flow rule, it is assumed that a, b, and C are not functions of stress. This procedure can be interpreted as using an associated flow rule with an error that is presumably small or as using a nonassociated flow rule. Third, the model does not use a limit surface. Instead, if a limit state is described as the point of maximum value of a measure of stress for a prescribed loading path, then the limit state is automatically predicted by the model and is path-dependent. Last, shear and tensile damage are incorporated but in an approximate sense since these failure mechanisms involve directional properties associated with crack and shear planes. However, for relatively simple states of stress (one dominant principal value for stress or strain) the model should be able to predict concrete behavior fairly accurately.

Since there is a very small amount of strain-rate data available to differentiate between possible features, only the simplest strain-rate formulation can be justified. The approach that is proposed consists of replacing H and a (= a_1, a_2) with H_D and a_D, respectively, where

$$H_D = H \left[1 + A_i \tanh \frac{\dot{e}^i}{\dot{e}_o} \right]$$

$$a_D = a \left[1 + A_i \tanh \frac{\dot{e}^i_v}{\dot{e}_o} \right]$$

(29)

55

In these relations $\dot{\bar{e}}_0$ denotes a reference strain rate and A_i is a dynamic amplitude parameter. With these modifications the theory goes through with no further changes.

EVALUATION

The experimental data in Reference 3 were used as the primary means for evaluating this model. Correct qualitative features were sought for a uni-axial tensile stress path, a hydrostatic stress path for relatively low pres-sures, and uniaxial compressive stress paths under three different initial confinement pressures. Material parameters for the model were taken to be

$$E = 4.1 \times 10^{10} \text{ Pa} (6.0 \times 10^5 \text{ lb/in}^2)$$

$$\nu = 0.18$$

$$\gamma = 0.9$$

$$\lambda = 2.8 \times 10^{10} \text{ Pa} (4.0 \times 10^6 \text{ lb/in}^2)$$

$$A_i = 1$$

$$\dot{\bar{e}}_0 = 0.5$$

with the following initial values also used:

$$A = 2.1 \times 10^6 \text{ Pa} (300 \text{ lb/in}^2)$$

$$A_0 = 2.2 \times 10^5 \text{ Pa} (315 \text{ lb/in}^2)$$

$$B = 2.1 \times 10^7 \text{ Pa} (-3000 \text{ lb/in}^2)$$

Theoretical and experimental response curves for hydrostatic compression are shown in Figure 24. Attempts to match experimental data were limited to the use of a secant modulus that varies with the confinement stress. Other models have used an analytical expression to provide a good comparison and such an approach could also be used with this model.
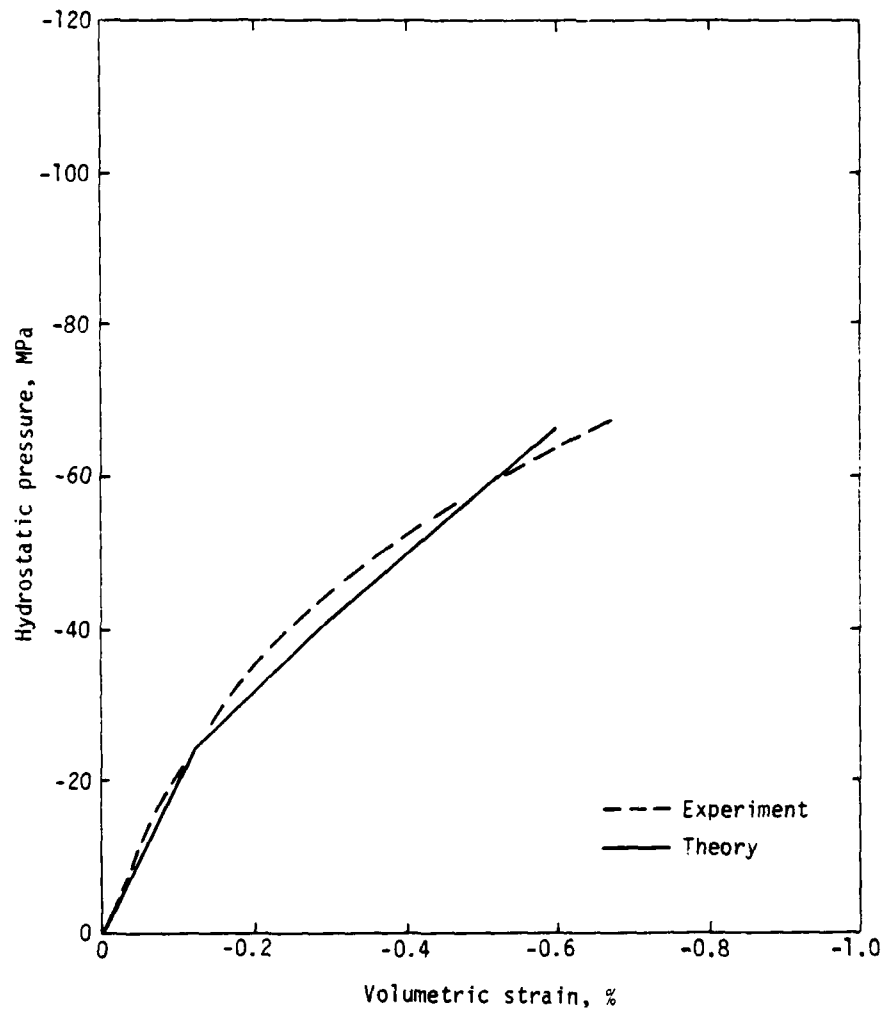
Figure 24. Hydrostatic experimental and analytical
response curves.

The uniaxial compressive stress curves were obtained with initial con-
finement pressures of 0, 6.9 x 10⁶ Pa (-1000 lb/in²), and 1.4 x 10⁷ Pa
(-2000 lb/in²). The nonzero stress is plotted as a function of the corre-
sponding strain in Figure 25a while confinement stress is shown as a function
of volumetric strain in Figure 25b. Since information concerning the lateral
strain is contained within these curves, separate plots involving lateral
strain are not given.

The result of uniaxial tensile stress load is shown in Figure 26.
Although the model provides a fairly sharp drop, the curve shows a subsequent
nonzero stress that has been included to provide numerical stability and that
does not reflect a physical phenomenon.

The effect of strain rate is shown in the typical uniaxial stress curves
of Figure 27 for various initial confining pressures. The nominal uniaxial
strain rates are shown in the figure. The uniaxial response indicates the
type of strength enhancement that is generally indicated by experimental data.
However, for cases involving an initial hydrostatic state of stress, the peak
stress associated with a specified strain rate is less than the peak stress
for no strain rate. The reason is that inelastic strain and damage is accu-
mulated less rapidly in the presence of a strain rate so that, for a given
uniaxial strain, the flow surface translates and expands at a slower rate.
Thus the implication of the analytical model is that for higher strain rates,
the material behaves more like a von Mises material since the limiting values
of effective shear stress are less dependent on mean pressure. It will be
difficult to devise an experiment that can verify such a conjecture.

This set of results is quite limited in extent. However, many important
concrete features are qualitatively reproduced by a rather elementary model.
This would indicate that the approach merits a more detailed investigation.
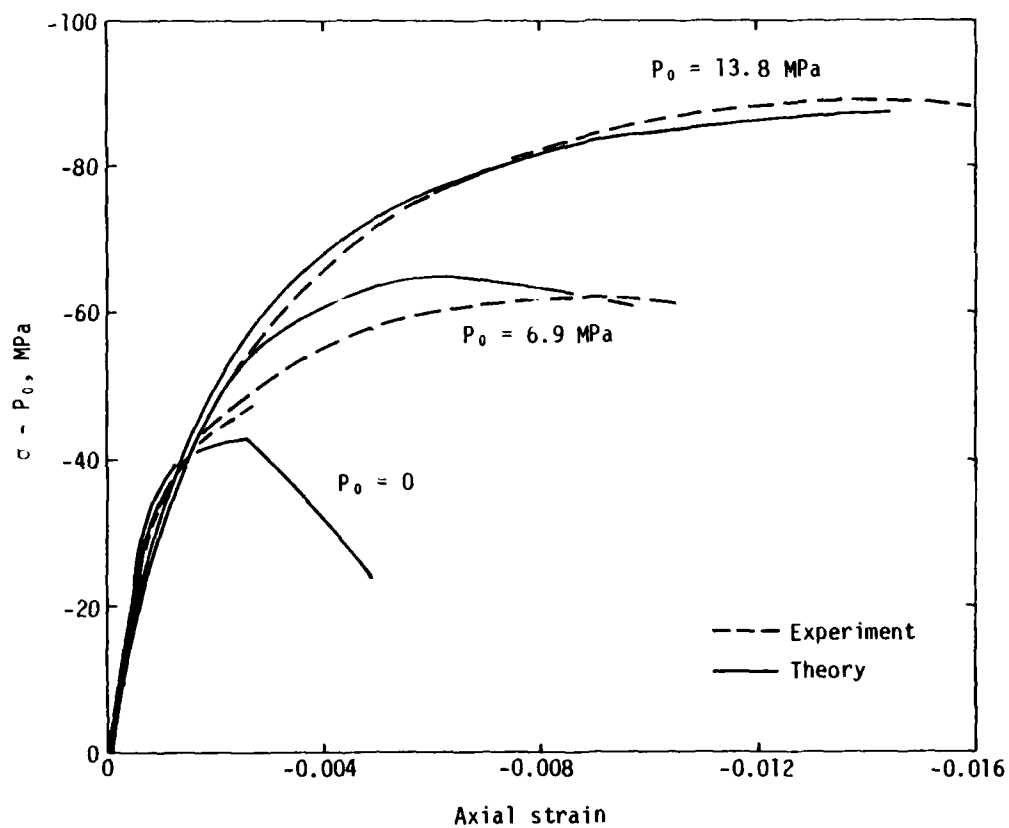
(a) Axial stress versus axial strain.

Figure 25.   Triaxial experimental and analytical response curves.
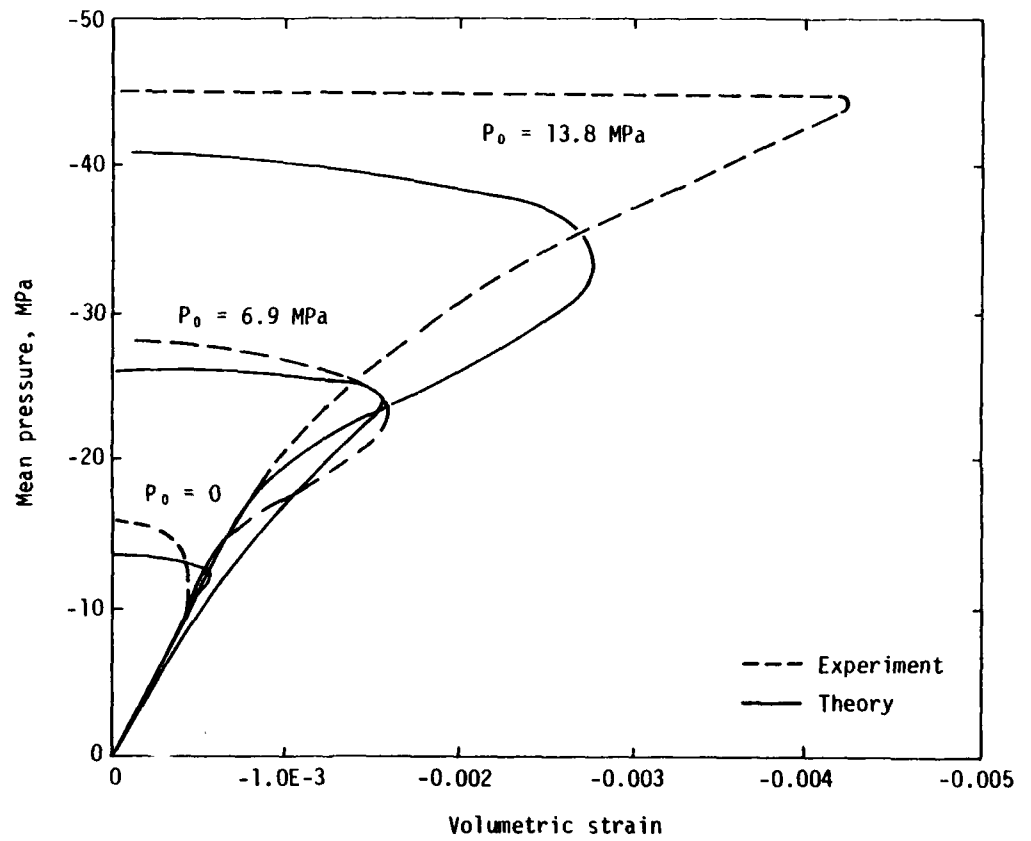
(b) Mean pressure versus volumetric strain.

Figure 25. Concluded.
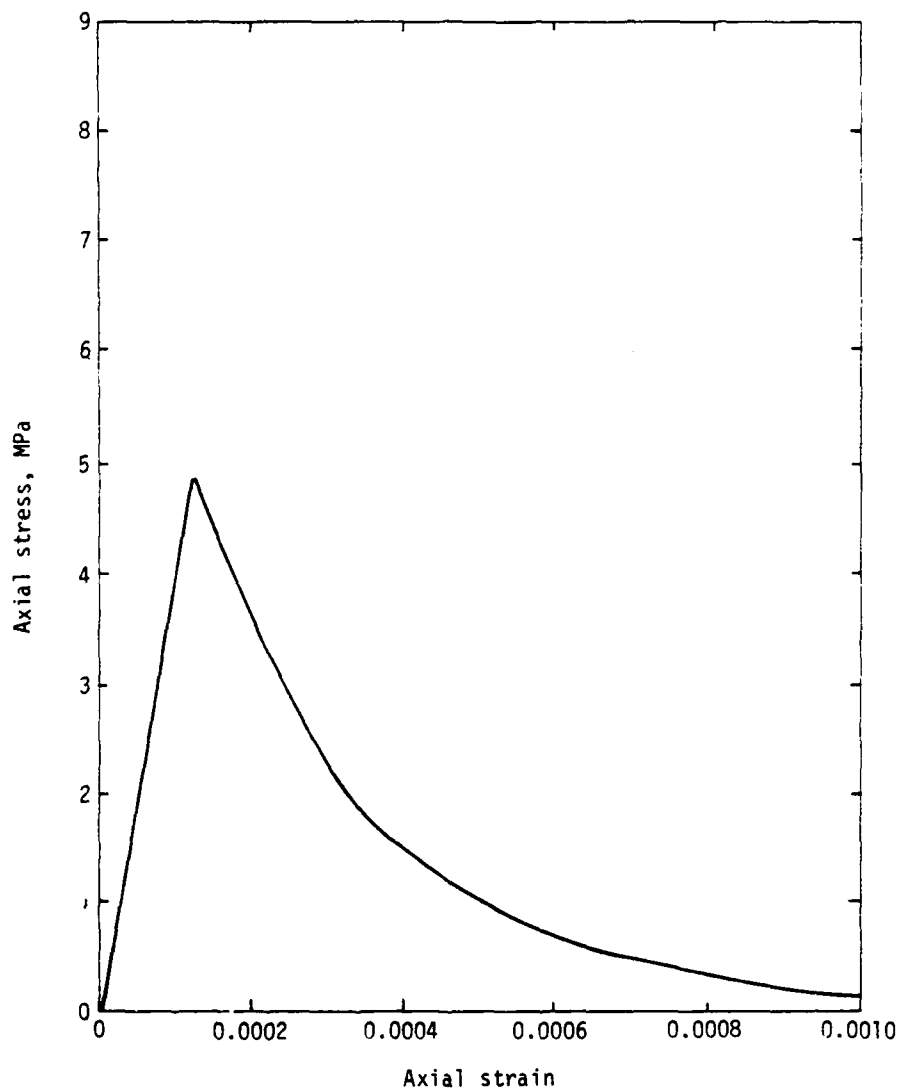
Figure 26. Analytical tensile response curve.
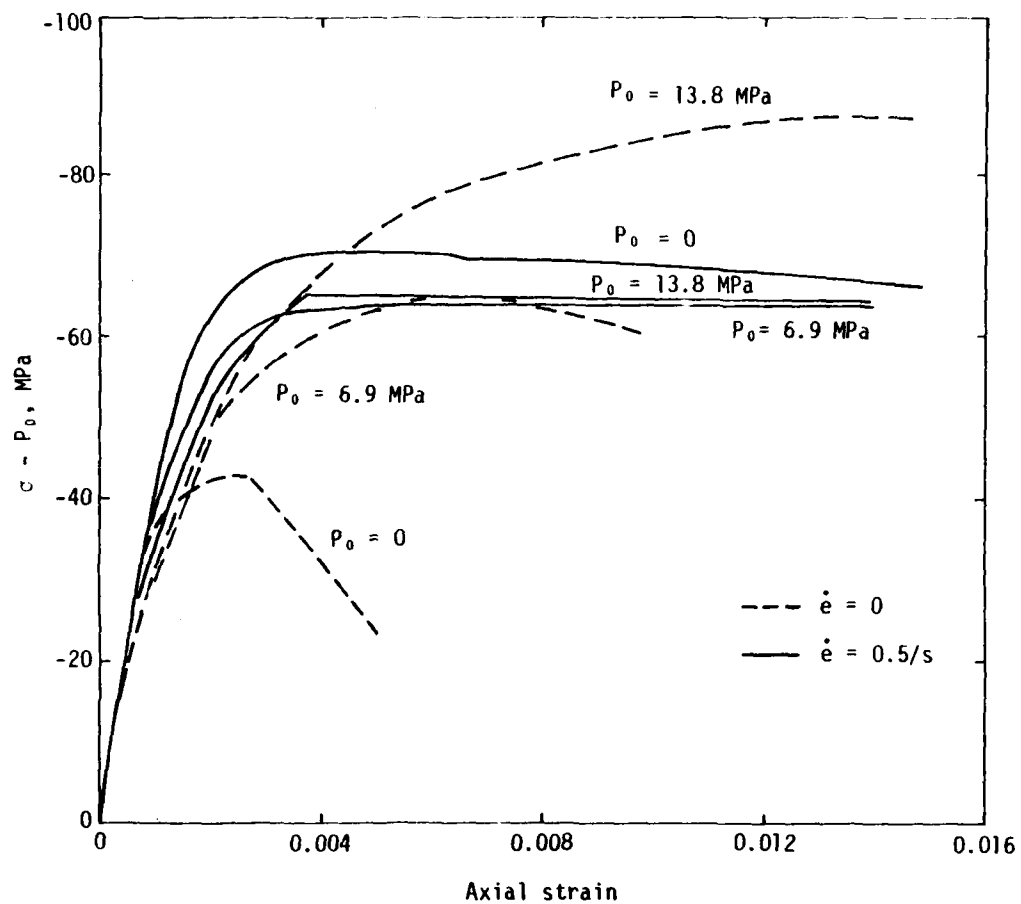
(a) Axial stress versus axial strain.

Figure 27. Triaxial response curves as a function of strain rate.
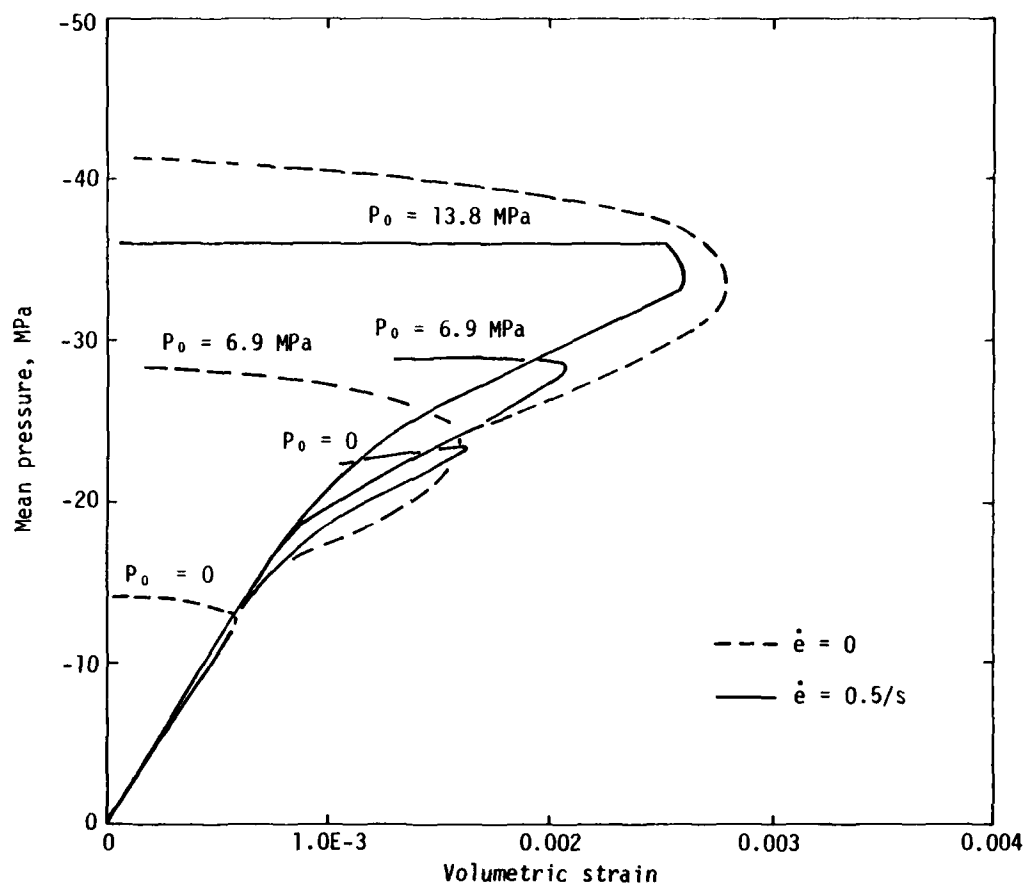
(b) Mean pressure versus volumetric strain.

Figure 27. Concluded.

POTENTIAL

With a relatively modest extension of classical plasticity theory, this model appears to properly display the following important features of concrete behavior:

• proper dilatation and ductility features near failure for a representative range of mean confinement pressures;

• shear enhanced compaction;

• the correct qualitative failure aspects for compression, shear and tension;

• a three-dimensional theory that displays interaction between shear and normal stress effects; and

• the capability to handle rate effects.

In the compressive regime, loss of strength can be modeled by reducing the values of γ or H. At this stage it is assumed that H should be reduced as a function of both shear and dilatational damage. The physical significance of reducing γ has not been fully explored.

No assumptions have been made that would restrict the theory to one or two dimensions. The theory is completely three-dimensional in nature and displays the general interaction of normal and shear stresses.

For dynamic loads that can provide strain rates of the order of 1/s, a constitutive model for concrete must be able to display rate effects. This model does so in a simple way by allowing the flow surface to expand with inelastic strain rate. All algorithms remain the same and so does the prediction of damage.

The viscoplastic model developed here has the unique capability of being able to simultaneously predict inelastic deformation, rate effects, and damage.

V. BEAM ANALYSIS

EXPERIMENTAL RESULTS

As part of a comprehensive effort to provide an experimental data base to be used for the verification of reinforced concrete constitutive models, a series of tests was performed on reinforced concrete beams subjected to lateral and axial forces (Ref. 29). The beams were loaded to collapse so that data from both the pre- and postlimit loading regimes are available. The loading system consisted of two symmetrically placed lateral forces that were displacement controlled and an axial force that was a fixed ratio of the ˉ .eral force. The test matrix included the following:

- monotonic loading to failure of a beam with shear reinforcement,

- monotonic loading to failure of a beam with no shear reinforcement, and

- cyclic loading to failure of a beam with shear reinforcement.

The general loading configuration and beam geometry are shown in Figures 28 and 29 respectively. A more detailed description of the loading apparatus, beam specifications, and material properties is given in Reference 29. Deflection, rotation, and strain measurements were taken at the stations indicated in Figures 30 and 31. Load cells were used to measure the lateral and axial forces applied to the beams.

Simultaneously with the beam testing program, conventional cylindrical static tests were performed to determine concrete strength. The concrete strength varied from 31 to 41 MPa and the corresponding maximum lateral load on the beam for all three tests showed a smaller variation with all cases falling in the range of 210 to 240 kN. The ratio of axial to lateral force varied from 3.0 to 3.4 for these tests.

ANALYTICAL MODEL

Since a working algorithm for each constitutive model was to be incorporated into the finite element code SAMSON II, it was decided to use this program to analyze the beam problems for which experimental data were available.

Lateral force (F)

| 1.30 m | 1.22 m | 1.30 m |

Axial load (P)

P

3.82 m
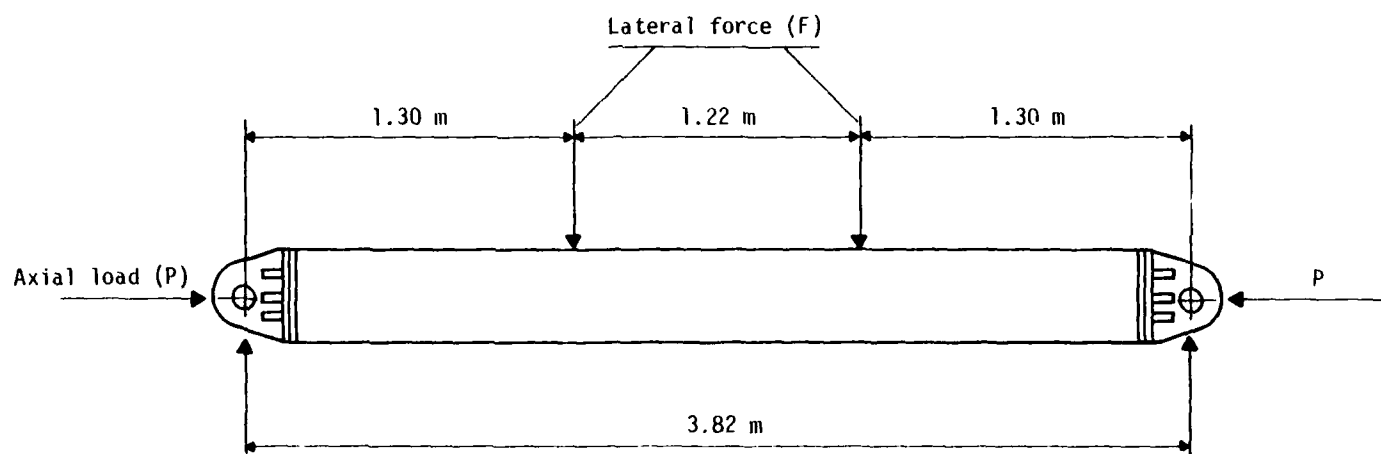
Figure 28. General loading configuration.

A ←──┤   3.82 m   ├──

(a) Elevation

229 mm

38 mm

Two No. 2 rebars

381 mm

No. 2 rebar stirrups at 152 mm
on center (except Series 2)

Three No. 6 rebars

64 mm

(b) Section A-A

114-mm radius

178 mm

Rebar

203 mm

Rebar anchor
loops 305 mm
long (welded to
end plate)

178 mm

100-mm diameter
shaft

Rebar
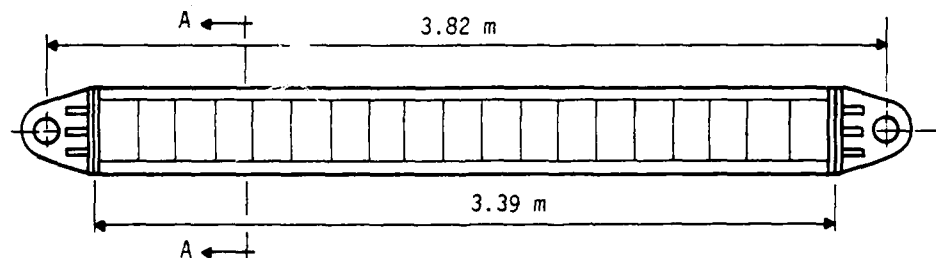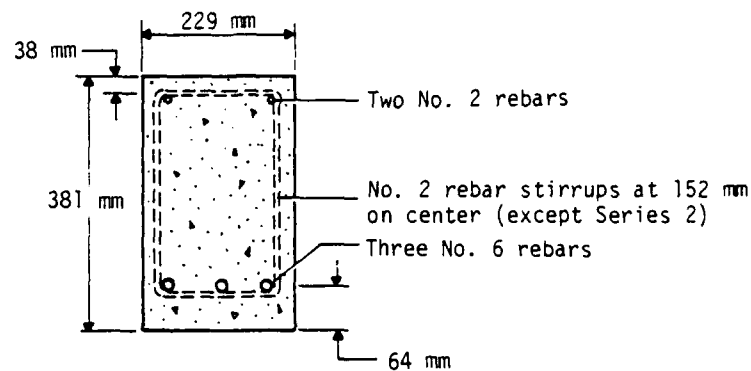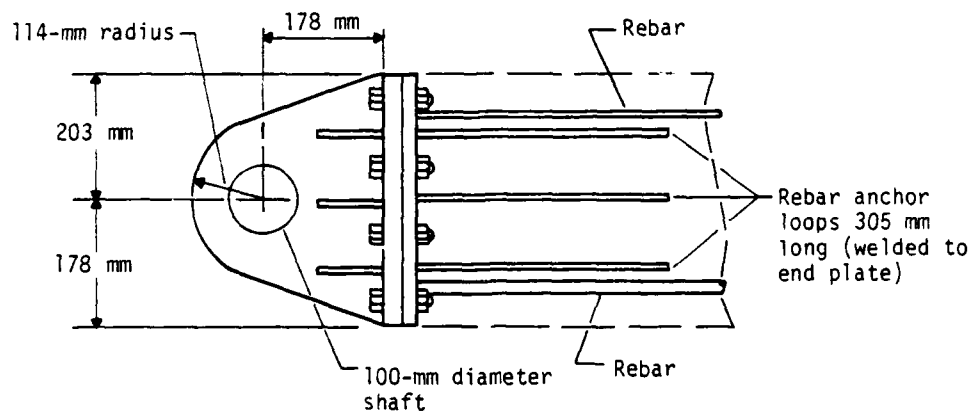
(c) End detail

Figure 29. Beam geometry.

67

Station numbers 0 1 2 3 4 5 6 7 8

270 mm ─── 419 mm ─── 419 mm ─── 270 mm

←2 x 610 mm = 1220 mm→←2 x 610 mm = 1220 mm→

─── 1.91 m ─── ─── '.91 m ───

─── 3.82 m ───

88
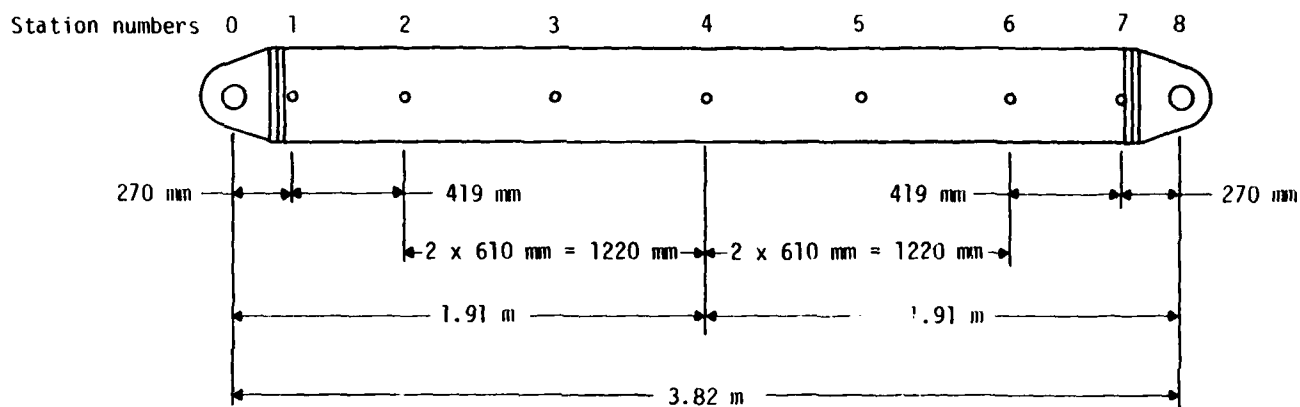
Measurements:
    Stations 0 and 8, horizo, tal and vertical displacement.
    Stations 1 and 7, rotation only.
    Stations 2 through 6, vertical deflection.
    Stations 2 through 6, strain (Fig. 33).

Figure 30. Measurement station layout

Station 2   Station 3   Station 4

Station 5   Station 6
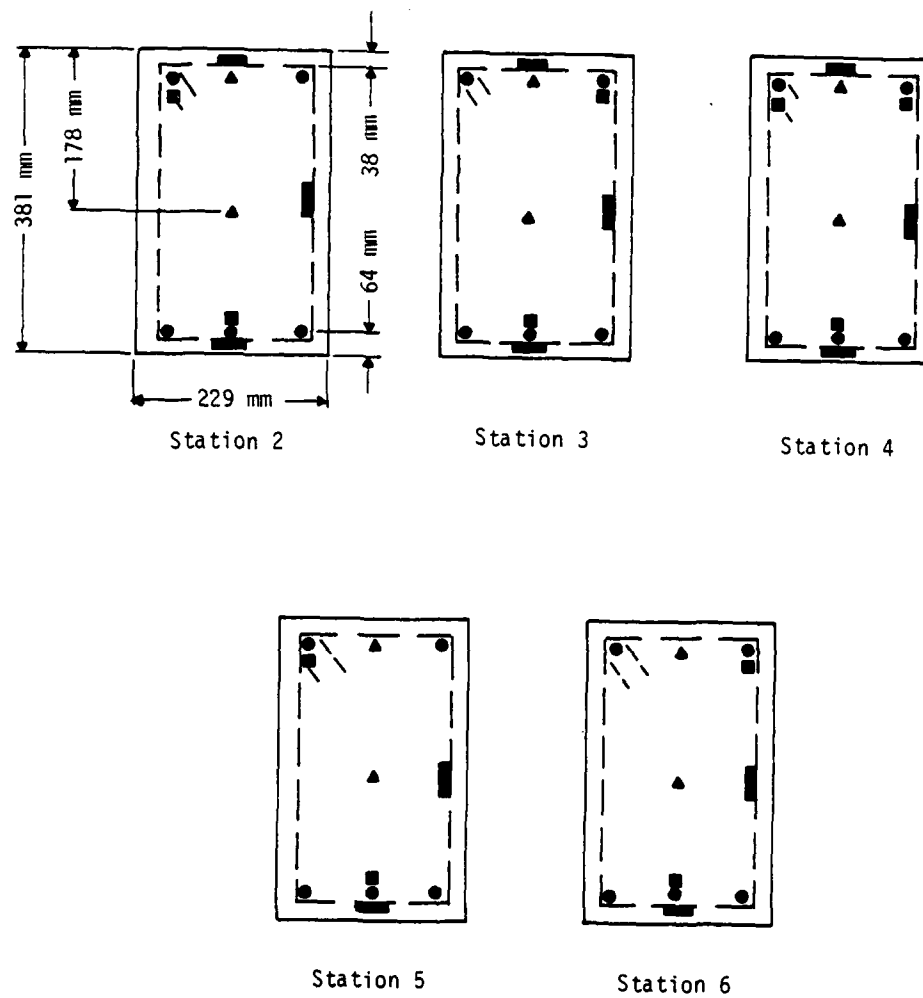
Legend

■ Longitudinal steel strain

▬ Vertical or transverse steel strain

▲ Embedded concrete strain

Figure 31. Strain measurement locations

69

The code is intended to be used primarily for dynamic problems although a
dynamic relaxation procedure is available for static problems. This procedure
involves the use of linear artificial viscosity as applied to element strain
rates. However, this approach appeared to be ineffective for a model beam
problem, so a temporary modification was made to SAMSON II to introduce nodal
damping. At each node a force is introduced that is proportional to the nodal
velocity but with opposite sign. The factor in this expression was also
assumed to be proportional to the difference in acceleration for successive
time steps. For a one-dimensional linear system with no forcing function,
this difference is proportional to the stiffness of the system. The net
result is a damping factor related to the critical damping term of a viscous
system.

The finite element model for the system is illustrated in Figure 32.
Element dimensions were chosen to provide a reasonable number of elements for
representing the variation in stress across the beam, to keep the aspect
ratios close to one, to have the points of load application at nodes, and to
have the tensile reinforcing steel lie along a line of nodes.

Because of symmetry only one-half of the beam can be modeled, with the
displacements of the nodes at the right end restricted to the vertical plane.
To provide vertical constraint to the model, node 49 at the left end is con-
strained to move horizontally.

The lateral forcing function consists of a monotonically increasing dis-
placement for node 107. In the experiment the force necessary to provide this
displacement was automatically monitored and an axial force equal to the lat-
eral force multiplied by approximately 3.2 was simultaneously applied. Since
this cannot be done analytically without some program modification, a simpli-
fied force-time function was used for the axial load. The lateral displace-
ment was applied analytically at the rate of 0.002 m/s with the maximum load
expected at a displacement of approximately 0.024 m or 0.012 s. The axial
force was applied as a triangular function, rising from zero to a peak value
of 800 kN at 0.012 s and decaying to zero at a time of 0.048 s. This axial

Figure 32. Finite element model for beam with no shear reinforcement

load definition was based on a presumed lateral force that behaved in the same manner but with a peak value of 240 kN. Thus the comparison of the predicted lateral force with the measured one is a measure of the overall accuracy of the analysis.

Point loads are difficult to handle with most constitutive models except for elastic ones. Thus the two elements adjacent to the applied lateral force and shown as a shaded area in Figure 32 were restricted to being elastic. The left end of the beam included a steel bracket as well as additional reinforcement, so it would be expected to exhibit more strength than other sections of the beam. This area is also shaded in Figure 32 and was treated as an elastic material.

All other rectangular elements represent plain concrete. The tensile and shear reinforcing steel were represented with bar elements. The tensile reinforcing steel and the vertical shear reinforcing steel were consolidated into a single set of elements with a cross-sectional area equal to that of the reinforcing steel. For the case of no shear reinforcement, these vertical bar elements were deleted and the assumption of plane stress was invoked. For the problem with shear reinforcement, the horizontal part of the steel was represented in an approximate manner by invoking conditions of plane strain rather than plane stress.

Typical response curves for the beam experiments are shown in Figures 33 and 34 which show lateral force as a function of the centerline deflection for monotonic loading. Figure 33 represents the beam with shear reinforcement where failure is by flexural tension. An elastic regime is indicated for a load up to approximately 10 percent of the limit load. The subsequent regime shows an inelastic hardening behavior, and after the limit load is reached, a softening aspect is displayed. These results show the tremendous energy-absorbing capacity that is available even after a limit state has been reached.

The corresponding result for beams with no shear reinforcement is shown in Figure 34. Up to the limit state the behavior is very similar to the previous case. However, for this case, once the limit state was reached, the

72
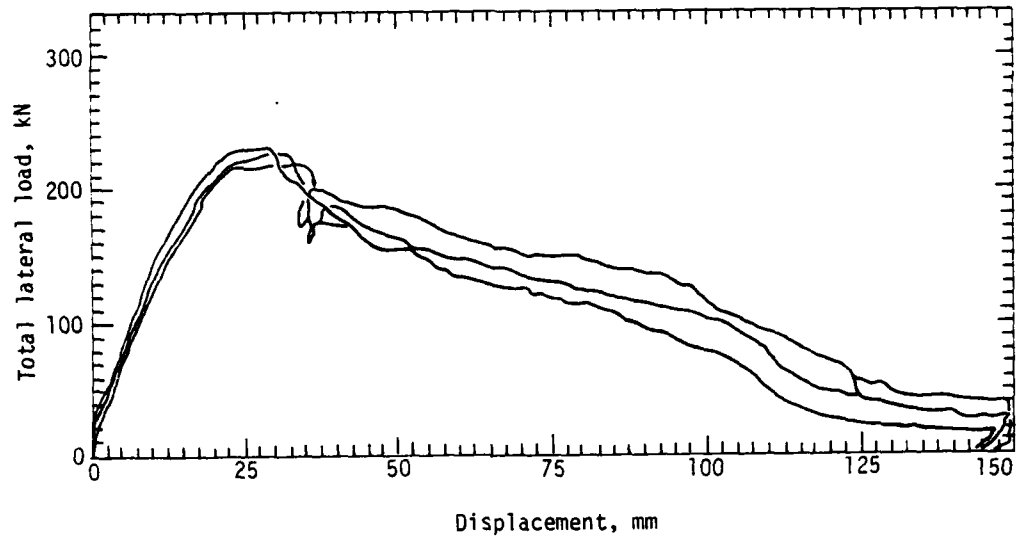
Figure 33. Load-centerline deflection for shear reinforced beam.
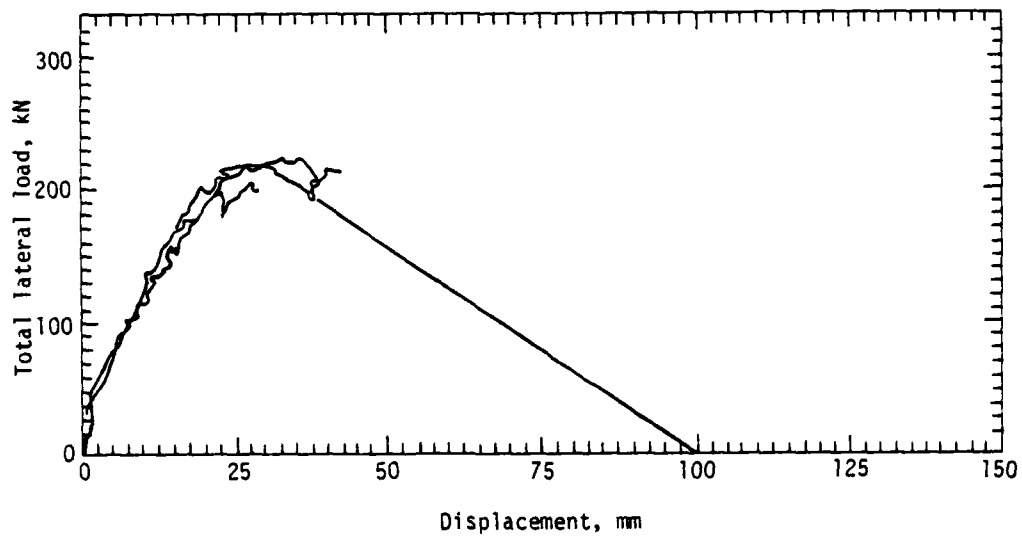
Figure 34. Load-centerline deflection for beam with no shear reinforcement.

73

tensile cracks extended into the compression zone and the beams collapsed.
The deflection load control system was not sensitive enough to prevent the
beam from abruptly transitioning to a failure state so the actual shape of the
postlimit curve is not known.

Experimental results for a structural member such as a beam cannot be
used to verify a three-dimensional constitutive model. However, if a contin-
uum analysis is performed on a beam, the comparison of predicted and experi-
mental data does provide a good indication of the adequacy of such models. If
the comparison is not good, presumably there is a fundamental reason for the
disagreement. If the comparison is good, this implies that a model is reason-
able but since all continuum response features are not exercised, the verifi-
cation is not complete.

To illustrate that the endochronic and viscoplastic models are opera-
tional and that numerical analyses can be performed, the next subsection out-
lines a finite element analysis of the monotonically loading cases for the
beams with and without shear reinforcement.

The reinforcing steel was modeled as an elastic-perfectly plastic mate-
rial with Young's modulus = 2.1×10^{11} Pa, Poisson's ratio = 0.27, and a yield
stress of 4.3×10^8 Pa. The shaded elements in Figure 32 were considered
elastic with Young's modulus = 2.0×10^{10} Pa and Poisson's ratio = 0.19 which
are consistent with the concrete. The corresponding material constants used
for the viscoplastic model were

$$\text{Young's modulus} = 2.0 \times 10^{10} \text{ Pa}$$

$$\text{Poisson's ratio} = 0.19$$

$$\lambda = 1.0 \times 10^{10} \text{ Pa}$$

$$\gamma = 1.0$$

$$A_i = 0$$

$$\dot{\bar{e}}_0 = 0$$

$$f_c' = 3.5 \times 10 \text{ Pa}$$

74

To define the initial state of the flow surface, the following values were used:

$$A = 2.0 \times 10^6 \text{ Pa}$$
$$A_0 = 2.2 \times 10^6 \text{ Pa}$$
$$B = -1.5 \times 10^7 \text{ Pa}$$

while the function H was defined as straight line segments between the strain and stress coordinate points $(0, 1.75 \times 10^7 \text{ Pa})$, $(0.0016, 1.75 \times 10^7 \text{ Pa})$, $(0.004, 1.0 \times 10^6 \text{ Pa})$, and $(2.0, 0)$.

The endochronic model defines variables in terms of f_c' $(3.5 \times 10^7 \text{ Pa})$ which greatly facilitates input. Additional required input was the density $(2320 \text{ N} - \text{s}^2/\text{m}^4)$ and a flag to indicate the state of stress (ISTRES = 2 for plane stress, ISTRES = 1 for plane strain).

ANALYTICAL RESULTS

If the analytical model is a reasonable representation of the experimental problem, two essential aspects should be displayed. First, the predicted limit load associated with the lateral loading mechanism should be close to the experimental values; and second, a qualitative representation of the softening feature of the load response curve is expected.

Modifications to the dynamic analysis code SAMSON II were necessary to handle this problem. The dynamic relaxation option did not appear functional so a change to incorporate a nodal viscous force was made. A test run using a strictly elastic material was performed for a prescribed lateral displacement which was increased monotonically to 0.025 m over a time span of 0.005 s and then fixed. After some exponentially decaying oscillations, a solution was obtained which appeared to agree with conventional elementary beam theory. Also, the resultant lateral force eventually converged to the reaction force at the left support in a time of 0.025 s which is approximately equal to the fundamental bending period of the elastic beam.

A similar approach was attempted with the use of the endochronic and vis-coplastic subroutines with the change that the lateral displacement was allowed to increase monotonically at the rate of 0.5 m/s. To avoid excessive computer costs, the restart capability of SAMSON II was used every 0.004 to 0.008 s and both models were run simultaneously. As the solution evolved, stress and strain comparisons were made and in general were consistent with each other and with what might be expected on an intuitive basis. However, after about 0.025 s of simulation it became apparent that values for the applied and support reaction lateral forces were not converging. It is specu-lated that the probable cause is the dynamic relaxation procedure in which case the displacement function would have to be specified as a ramp followed by a constant value to allow convergence, another ramp, and so on. However, each step could take approximately 0.025 s of simulation time to obtain a solution which would result in a fairly expensive procedure.

At the time that this approach was going to be attempted, all files were lost due to a hardware failure. At the time of this report, the various con-stitutive equation algorithms were just being recreated and a solution was not available.

VI. CONCLUSIONS

The endochronic concrete model has demonstrated an ability to model all the significant aspects of compressive concrete behavior except strain rate effects. It must be meshed with a cracking model for applications where tensile/cracking behavior is expected to be significant. The model produces inelastic behavior for all loadings in the deviatoric plane, unlike conventional models which utilize a loading surface. The endochronic model is believed to be closer to concrete behavior in this respect. The intrinsic time term used to define inelastic behavior provides what appears to be a logical avenue for the introduction of strain rate effects into the material model. In general, adjustments of the model to different concretes can be done easily. The large number of stored parameters and the nonlinearity of the formulation are computational disadvantages of the model.

Several qualitatively correct features are displayed by the viscoplastic model. For inelastic deformations these include shear enhanced compaction, other shear and normal strain interactions, and a large degree of ductility accompanied by dilatation for the case of an initial hydrostatic stress. Shear and tensile fracture modes are displayed although they are currently restricted to an isotropic description. Furthermore, enhanced uniaxial strength due to rate effects is automatically incorporated in the model. The combination of a relatively broad scope, simplicity, mathematical tractability, and reasonable predictive capability over a wide range of applications give this model a potential capability that is unique.

VII. RECOMMENDATIONS

The algorithm developed for the endochronic model produces a satisfactory representation of the results of uniaxial, biaxial, triaxial, and cyclic behavior of concrete. The model has been meshed with a tensile/cracking model and inserted into the SAMSON II structural analysis code. Continued evaluation of the model should involve investigations pertaining to its limitations, capabilities, and potential.

1. Checkout of the algorithm was done by making comparisons with data presented in the description of the model, i.e., data which were used in a curve fitting program to determine the parameters involved in the model. Similar comparisons should be made with the other concrete data, such as that developed at New Mexico State University. Comparisons with data involving stress paths with a significant component in the direction tangent to the failure surface would be of particular interest. The two alternate adjustment methods for fitting the model to a concrete should be evaluated if appropriate data are available.

2. The algorithm should be studied to determine, if possible,

- under what conditions may the nonlinear analysis prove unstable,
- to what extent does the tensile model influence the endochronic (compressive) model,
- to what extent can efficiency be improved by taking such action as considering an alternate cracking model or using approximations or combinations to reduce the number of stored parameters, and
- what changes are needed to make the model completely three dimensional.

3. An attractive feature of the endochronic model is its apparent suitability for the introduction of strain rate effects. It is recommended that pursuit of this goal be initiated.

4. The ultimate goal of the modeling work is to provide a means of modeling reinforced concrete, a material with multiple idiosyncracies, only one of which is the behavior of plain concrete. The endochronic model should be used in combination with existing models of reinforced concrete behavioral

features such as debonding and dowel action to evaluate the capability to model the behavior of a simple reinforced concrete specimen. This study may lead to the incorporation of some of these features into an endochronic reinforced concrete model.

The viscoplastic model has been developed to the point that correct characteristic response features are displayed. Also, initial functional forms have been chosen for describing the motion of the ellipse, but for a limited range of parameters (for example, hydrostatic pressure). A degree-of-failure-mode description and rate effects have been incorporated. However, there is a significant amount of detailed information that is still missing. The following investigations are necessary to fully develop the model:

1. Further numerical studies concerning parameters and evolution functions are required. For example, a completely analytical expression should be used to represent purely hydrostatic response. A better way must be developed for relating ellipse parameters to f_c', and the description of the implicit assumptions used to describe isotropic failure must be improved. Reasonably detailed comparisons with recent experimental data from New Mexico State University should be made.

2. The failure modes associated with the viscoplastic model are isotropic. Shear and tensile fracture have directional properties that are fully reflected in a discrete cracking model. These are two extreme methods for describing failure and the degree of complexity varies accordingly. It is possible that an intermediate approach involving an extension of the flow model to incorporate anisotropy might yield a relatively simple but useful way for representing fracture. At least a limited investigation should be worthwhile.

3. Several new features have been incorporated into the viscoplastic model. Although they appear to be necessary to represent experimental data, there is still a question of how these features affect the prediction of the response of components such as beams, columns, plates, and shells. A numerical investigation of typical static and dynamic loadings on such components in which different models are used might be very illuminating.

80

4. A large number of problems of interest to the Air Force involves rate
effects. A thorough investigation of the strain-rate part of the viscoplastic
model including component behavior should be performed. Simultaneously,
dynamic experiments on concrete specimens and components should be performed
to see if predicted responses are even qualitatively correct for analyses.

5. The modeling of reinforced concrete including the failure modes that
involve debonding and dowel action is essential for any reasonable analytical
technique. Partial reductions in strength are relatively easy to incorporate
into the viscoplastic model but to do this in a sensible manner is a difficult
task. A simultaneous investigation of cubical specimens with embedded steel
rods would be extremely helpful.

6. The use of dilatation as a measure of damage has been suggested in
Reference 30. The use of a model that can predict dilatation reasonably
accurately opens the possibility of closer evaluation of the concept. New
load paths including more than one principal stress in tension, complex
reversals in the compressive regime, and cyclic loading should be considered.

REFERENCES

1. Sinha, B. P., Gerstle, K. H., and Tulin, L. G., "Stress-Strain Relations for Concrete Under Cyclic Loading," *Journal of the American Concrete Institute*, Vol. 61, No. 2, February 1964, pp. 195-210.

2. Kupfer, H., Hilsdorf, H. K., and Riisch, H., "Behavior of Concrete Under Biaxial Stresses," *Journal of the American Concrete Institute*, Vol. 66, August 1969, pp. 656-666.

3. Green, S. J., and Swanson, S. R., *Static Constitutive Relations for Concrete*, AFWL-TR-72-244, Air Force Weapons Laboratory, Kirtland Air Force Base, New Mexico, April 1973.

4. Hsieh, S. S., Ting, E. C., and Chen, W. F., *A Plastic-Fracture Model for Concrete - Part I: Theory*, Report CE-STR-80-14, School of Civil Engineering, Purdue University, August 1980.

5. Watstein, D., "Effect of Straining Rate on the Compressive Strength and Elastic Properties of Concrete," *Journal of the American Concrete Institute*, Vol. 24, April 1953, pp. 729-744.

6. Drucker, D. C., "A More Fundamental Approach to Plastic Stress-Strain Relations," *Proceedings, 1st U.S. National Congress of Applied Mechanics*, American Society of Mechanical Engineers, New York, 1951, pp. 487-491.

7. Chen, W. F., and Suzuki, H., "Constitutive Models for Concrete," *Computers and Structures*, Vol. 12, 1980, pp. 23-32.

8. Bazant, Z. P., and Kim, S. S., "Plastic-Fracturing Theory for Concrete," *Journal of the Engineering Mechanics Division*, American Society of Civil Engineers, Vol. 105, No. EM3, Proceedings Paper 14653, June 1979, pp. 407-428.

9. Murray, D. W., Chitmuyanondh, L., Rijub-Agha, K. Y., and Wong, C., "Concrete Plasticity Theory for Biaxial Stress Analysis," *Journal of the Engineering Mechanics Division*, American Society of Civil Engineers, Vol. 105, No. EM6, Proceedings Paper 15046, December 1979, pp. 989-1006.

10. Dragon, A., and Mroz, Z., "A Continuum Model for Plastic-Brittle Behaviour of Rock and Concrete," *International Journal of Engineering Science*, Vol. 17, 1979, pp. 121-137.

11. Willam, K. J., and Warnke, E. P., "Constitutive Model for the Triaxial Behavior of Concrete," Proceedings, International Association of Bridge and Structural Engineers Seminar on Concrete Structures Subjected to Triaxial Stresses, Paper III-1, published in *Proceedings*, Vol. 19, pp. 1-17 (1975), Bergamo, Italy, May 17-19, 1974.

12. Drucker, D. C., Gibson, R. E., and Henkel, D. J., "Soil Mechanics and Work Hardening Theories of Plasticity," *Transactions*, American Society of Civil Engineers, Vol. 124, Paper No. 2864, 1957, pp. 338-346.

13. Lade, P. V., "Three-Parameter Failure Criterion for Concrete," submitted for publication to *Journal of the Engineering Mechanics Division*, American Society of Civil Engineers.

14. Lade, P. V., "Elasto-Plastic Stress-Strain Theory for Cohesionless Soil with Curved Yield Surfaces," *International Journal of Solids and Structures*, Vol. 13, November 1977, pp. 1019-1035.

15. Cedolin, L. C., Yves, R. J., and Dei Poli, S., "Triaxial Stress-Strain Relationship for Concrete," *Journal of the Engineering Mechanics Division*, American Society of Civil Engineers, Vol. 103, No. EM3, Proceedings Paper 12969, June 1977, pp. 423-439.

16. Ahmad, S., and Shah, S. P., *Complete Triaxial Stress-Strain Curves for Concrete*, College of Engineering, University of Illinois at Chicago Circle, March 1981.

17. Coon, M. D., and Evans, R. J., "Incremental Constitutive Laws and Their Associated Failure Criteria with Application to Plain Concrete," *International Journal of Solids and Structures*, Vol. 8, 1972, pp. 1169-1180.

18. Elwi, A. A., and Murray, D. W., "A 3D Hypoelastic Concrete Constitutive Relationship," *Journal of the Engineering Mechanics Division*, American Society of Civil Engineers, Vol. 105, No. EM4, Proceedings Paper 14746, August 1979, pp. 623-641.

19. Bazant, Z. P., Discussion of Reference 18, *Journal of the Engineering Mechanics Division*, American Society of Civil Engineers, Vol. 106, No. EM2, April 1980, pp. 422-423.

20. Elwi, A. A., and Murray, D. W., Response to Reference 19, *Journal of the Engineering Mechanics Division*, American Society of Civil Engineers, Vol. 107, No. EM2, April 1980, pp. 435-437.

21. Bazant, Z. P., and Bhat, P., "Endochronic Theory of Inelasticity and Failure of Concrete," *Journal of the Engineering Mechanics Division*, American Society of Civil Engineers, Vol. 102, No. EM4, Proceedings Paper 12360, August 1976, pp. 701-722.

22. Bazant, Z. P., and Schieh, C. L., "Endochronic Model for Nonlinear Tri-axial Behavior of Concrete," *Nuclear Engineering and Design*, Vol. 47, 1978, pp. 305-315.

23. Bazant, Z. P., "Endochronic Inelasticity and Incremental Plasticity," *International Journal of Solids and Structures*, Vol. 14, No. 9, September 1978, pp. 691-714.

24. Bazant, A. P., and Schieh, C. L., "Hysteretic Fracturing Endochronic Theory for Concrete," *Journal of the Engineering Mechanics Division*, American Society of Civil Engineers, Vol. 106, No. EM5, Proceedings Paper 15781, October 1980, pp. 929-950.

25. Cheverton, K. J., *Reinforced Concrete Models Evaluation for NX Shelter Hardness and Survivability*, Final Report SSS-R-81-473, Systems, Science and Software, November 1980.

26. Cedolin, L., and Dei Poli, S., "Finite Element Studies of Shear-Critical R/C Beams," *Journal of the Engineering Mechanics Division*, American Society of Civil Engineers, Vol. 103, No. EM3, Proceedings Paper 12968, June 1977, pp. 395-410.

27. Fardis, M. N., and Buyukozturk, O., "Shear Transfer Model for Reinforced Concrete," *Journal of the Engineering Mechanics Division*, American Society of Civil Engineers, Vol. 105, No. EM2, Proceedings Paper 14507, April 1979, pp. 255-275.

28. Schickert, G., and Winkler, H., "Results of Tests Concerning Strength and Strain of Concrete Subjected to Multiaxial Compressive Stresses," *Bundesanstalt für Materialprüfung*, Bericht No. 46, May 1977, West Berlin, Germany.

29. Lane, G. E., *Reinforced Concrete Beams Under Combined Axial and Lateral Loading*, AFWL-TR-81-99, Air Force Weapons Laboratory, Kirtland Air Force Base, New Mexico, January 1982.

30. Traina, L. A., and Jeragh, A. M. A., *Fatigue of Plain Concrete Subjected to Biaxial-Cyclical Loading*, Paper presented at the 1930 Fall Convention, American Concrete Institute, San Juan, Puerto Rico.

SYMBOLS

A_o tensile limiting value for A

A_i amplitude of strain rate-dependent part of plasticity function

A, B coordinates of intercept points for ellipse in viscoplastic models

C P-coordinate of the horizontal tangent point for the visco-plastic model

$\underset{\sim}{C}$ elasticity tensor

F_1, F_2 invariant functions of stress, strain, and ξ in endochronic model

G elastic shear modulus

H intercept of shear line on $\overline{J}$-axis viscoplastic model

$\underset{\sim}{I}$ identity tensor

I_1 first stress invariant

J_2' second deviatoric stress invariant

P mean pressure (-1/3 tr $\underset{\sim}{\sigma}$)

P_o hydrostatic pressure

a major axis length of ellipse in viscoplastic model

a_1, a_2 major axis lengths of the two ellipses used in viscoplastic model

b minor axis length of ellipse in viscoplastic model

c coefficient defining the loading condition in endochronic model

d horizontal tangent point of ellipse in viscoplastic model

$\overline{e}$ inelastic strain deviator

$\underset{\sim}{e}$ total strain tensor

e_{kk} volumetric strain

e_o — strain at hydrostatic confining pressure

$\dot{\bar{e}}_o$ — reference strain rate

$\bar{e}^*$ — strain measure of damage

$\underset{\sim}{e}^d$ — deviatoric strain tensor

$\underset{\sim}{e}^{*d}$ — *adjusted deviatoric strain tensor in endochronic model*

$\underset{\sim}{e}^{d(fr)}$ — fracturing deviatoric inelastic strain tensor in endochronic model

$\underset{\sim}{e}^{d(pl)}$ — plastic deviatoric inelastic strain tensor in endochronic model

$\underset{\sim}{e}^e$ — elastic strain tensor

$\underset{\sim}{e}^i$ — inelastic strain tensor

e_v^i — inelastic volume change

f_c' — ultimate compressive strength of standard cylinder

f_t — uniaxial tensile strength

$\underset{\sim}{g}$ — ɔ stress gradient of plasticity function

tr — trace operator

$(\dot{\ })$ — differentiation with respect to time

λ — initial inelastic modulus

$\lambda_{ij}, \lambda_{ij}'$ — jump-kinematic hardening parameters in endochronic model

λ_s — secant modulus

β — parameter used in viscoplastic algorithm

γ — slope of shear line in viscoplastic model

ζ — plastic intrinsic time parameter in endochronic model

η_1, η_2 — parameters used in viscoplastic algorithm

κ — fracturing intrinsic time parameter in endochronic model

λ — monotonically increasing scalar function in viscoplastic model

ν — Poisson's ratio

$\underline{\xi}$	deviatoric strain path length
$\underline{\xi}'$	volumetric strain path length
$\overline{\sigma}$	effective stress $(\sqrt{3}\ \overline{\sigma}_s)$
$\underset{\sim}{\sigma}$	Cauchy stress tensor
$\underset{\sim}{\sigma}^d$	stress deviator tensor
$\underset{\sim}{\sigma}^{*d}$	adjusted stress deviator tensor in endochronic model
σ_s	equivalent shear stress $(\sqrt{J_2'})$
τ_o	octahedral shear stress
Ω	plasticity function in viscoplastic model